Prifysgol Abertawe
Swansea University

Dual-Energy X-ray Absorptiometry (DEXA) as an Instrument for Assessing Bone Mineral Density in Historic Human Remains

Frederick Louis Evans (BSc Hons)

Submitted to Swansea University in fulfilment of the requirements for the Degree of Master of Science by Research

Swansea University

2023

Abstract

Dual-energy X-ray absorptiometry (DEXA) is the gold standard, non-invasive method for the measurement of bone mineral density (BMD). DEXA measures BMD using two X-ray beams of different energies. These beams are attenuated differently by bone and soft tissue, allowing for the determination of BMD. DEXA requires the presence of soft tissue and bone to measure BMD, but if a soft tissue proxy (STP), such as rice or gelatin, is used - DEXA can be used to scan human remains, specifically bones. The purpose of this study was twofold: develop a criterion method to measure BMD, using DEXA on historical human remains, then use the criterion method to investigate bilateral asymmetry and agreement (test re-test reliability) in a sample of historic human remains, specifically paired radii from the Mary Rose Trust's collection of fairly complete skeletons (FCS). The study developed a criterion method initially, by testing the efficacy, in terms of reliability, of using a suspension bracket to position the radius in a consistent position. Machine capability was tested by DEXA scanning one radius 16 times without moving it and using these values to calculate precision error. Method capability was tested by scanning one radius 16 times, removing it and replacing between scans, and using these values to calculate precision error. Once the optimum method of positioning samples was established, the optimum STP was determined. To determine optimum STP, the machine capability of dry rice was compared to that of differing concentrations of gelatin. Upon determination of the criterion method for measuring BMD using DEXA on historic human remains, agreement and bilateral asymmetry of BMD was measured in a population of 20 pairs of radii. This was done for samples in pronated and supinated orientation. Significant differences were tested for between dominant and non-dominant arm BMD (dominant arm being assumed as the arm with higher BMD). The criterion method for measurement of BMD using DEXA within historic human remains was found to be the use of a suspension bracket to position the sample with 11.7% gelatin blocks as an STP. This method resulted in a mean ± standard error of the mean (SEM) of 0.751±0.00028 mass/cm^2 (±0.037%), compared to the rice bed method (no suspension bracket and dry rice as an STP) which resulted in a mean ± SEM of 0.795±0.0015 mass/cm^2 (±0.19%). Once established, the criterion method was applied to the full sample of 20 pairs of radii to establish reliability and bilateral asymmetry. Reliability was assessed using Bland and Altman limits of agreement

(LOA) analysis which produced a sample mean = 0.762 mass/cm2, a systematic bias = 0.002 mass/cm2 (0.03%), upper LOA = 0.003 mass/cm2 (0.39%) and lower LOA = -0.0026 mass/cm2 (-0.34%). Significant differences were observed in pronated BMD, supinated BMD, and combined BMD values between dominant/non-dominant arm radii ($p < 0.05$, pronated: $p = 0.018$, supinated: $p = 0.019$, combined: $p = 0.018$). Of the 20 pairs of radii compared, 5 had bilateral asymmetry of BMD > 10% with the largest difference being 46.2%. To conclude, the criterion method for measuring BMD using DEXA on historic human remains is to position samples using a suspension bracket and use 11.7% gelatin blocks as an STP. Additionally, significant bilateral asymmetry was observed between dominant and non-dominant arm BMD in a population of 20 pairs of radii.

Declarations

This work has not previously been accepted in substance for any degree and is not being concurrently submitted in candidature for any degree.

Signed [redacted]

Date.....11/12/2023.....

This thesis is the result of my own investigations, except where otherwise stated. Other sources are acknowledged by footnotes giving explicit references. A bibliography is appended.

Signed [redacted]

Date..... 11/12/2023.....

I hereby give consent for my thesis, if accepted, to be available for electronic sharing

Signed [redacted]

Date..... 11/12/2023.....

The University's ethical procedures have been followed and, where appropriate, that ethical approval has been granted.

Signed [redacted]

Date..... 11/12/2023.....

Contents Page

Acknowledgements

Firstly, I would like to thank and acknowledge my supervisors, Dr Nicholas Owen, and Dr Shane Heffernan. The support and expertise provided throughout my research has been invaluable, and without their assistance, I would have found this project far more difficult.

Second, I would like to express my gratitude to the Mary Rose Trust and Dr Alex Hildred for providing the skeletal materials, without which, this truly unique and fascinating study would not have been possible.

Finally, I would like to thank my friends and family for the endless support and encouragement they provided me over the past two years – without which, none of this would have been possible.

List of Tables

Table 4.2.2. Table describing percentage difference in bone mineral density (BMD) between dominant and non-dominant radii for combined BMD values.

List of Figures

Abbreviations

BMD = Bone Mineral Density

DEXA = Dual -Energy X-ray Absorptiometry

G/cm^2 = Grams per Centimetre Squared

FCS = Fairly complete Skeleton

LA = Longitudinal Axis

Mass/cm^2 = Mass per Centimetre Squared

ROI = Region of Interest

SD = Standard Deviation

SEM = Standard Error of the Mean

STP = Soft Tissue Proxy

Equations

Chapter 1

Introduction

1.1. History of the Mary Rose

1.2. Dual-Energy X-Ray Absorptiometry (DEXA)

1.3. Bone Adaptation

1.4. Gelatin

1.5. DEXA with Historic Human Remains

1.6. Research Proposal

1. Introduction

1.1: History of the Mary Rose

The warship Mary Rose was an English carrack-type vessel and the flagship of King Henry VIII's Royal Fleet. Carracks were a class of sailing ship that predominantly saw service between the 14th-17th centuries. Carracks were typically built with three masts; however, some larger ships were outfitted with a fourth mast located behind the mizzenmast. Some of the largest carracks would have been up to 45 metres in length and had displacements of up to 1,000 tons (Britannica, 2016) (Tikkanen, 2021) (The History of the Mary Rose, 2021).

The first reference to the Mary Rose was in 1510 in a letter ordering the construction of "two new ships". Whilst not specifically named, these two ships were to be the Mary Rose and the Peter Pomegranate (sister ship to the Mary Rose). The Mary Rose was of a state-of-the-art design - 600 tons and designed to carry 6-8 large guns (The History of the Mary Rose, 2021).

In 1536, after 24 years of service in several campaigns against the French, the Mary Rose underwent a refit. Her refit saw extra gunports added, and in order to accommodate for this extra weight, her sides were strengthened. It is thought that the alterations made to the Mary Rose may have affected her sailing capabilities - a report by Vice-Admiral John Dudley in 1537 stated that some of the ships in the fleet were "unweatherly" in particular, it was noted that the ship "that Mr Carew is in" was particularly bad. Whilst it is unclear which ship "Mr Carew" was on at the time, it is known that George Carew was in command of the Mary Rose 8 years later - potentially indicating that the problematic ship noted by John Dudley was in fact the Mary Rose (Tikkanen, 2021) (The History of the Mary Rose, 2021) (Marsden, 2015).

On the 19th July, 1545, the Mary Rose left her anchorage in Portsmouth in order to engage the French fleet that had entered the Solent Estuary. Spanish Ambassador Francois van der Delft - an eyewitness to the battle of the Solent reported that after firing a volley from her port side guns, the Mary Rose turned and "heeled over with the wind". The ship dipped below the waterline, resulting in rapid flooding and ultimately the ship sank within a few minutes. It is estimated that of the ~500 strong

crew, no more than 35 survived the sinking (Tikkanen, 2021) (The History of the Mary Rose, 2021).

Due to the lack of eyewitness accounts, the exact cause of the Mary Rose's sinking is still unknown. Despite this, there are several theories that hold merit. Contemporary accounts suggested that the Mary Rose sank after coming under fire from French Galleys. This theory seemed plausible due to the ability of the Galley's armaments to cause extensive damage. Additionally, Martin du Bellay, a French nobleman and cavalry officer who was present at the battle of the Solent, claimed that the Mary Rose had been sunk by French guns. Despite these claims, this theory was largely disproved upon excavation of the wreck. Archaeologists who examined the wreck found no evidence to suggest the Mary Rose had experienced any extensive damage from gunfire (Bell et al., 2009) (Why Did the Mary Rose Sink?, 2021).

The most common, modern theory suggests the Mary Rose sank whilst performing an about turn manoeuvre. As she turned, she listed low on her starboard side, water flooded into the unsecured gunports - resulting in the ship's rapid sinking. This poorly performed manoeuvre could have been the result of several factors, including: the ship being overloaded and difficult to handle after the refits, an inexperienced crew, and an epidemic of dysentery in Portsmouth which may have hindered the crew's ability to effectively handle the ship (Bell et al., 2009) (Why Did the Mary Rose Sink?, 2021).

Despite having seen 34 years of service and being considered an older ship, the Mary Rose was still a valuable asset and as such her recovery was important. In the days after the sinking, a salvage attempt was commissioned by the then Secretary of State - William Paget. Charles Brandon, brother-in-law to King Henry VIII, took charge of the operation. In conjunction with Venetian salvagers, a traditional recovery method was employed. Divers were sent to the seabed to run cables under the ship's hull, these cables would then be attached to larger ships on the surface. These larger ships would then sail apart, pulling the cables taut and raising the stricken vessel to the surface. Once at the surface, the Mary Rose was to be led to shallower waters where she could be emptied of her contents and have the water pumped out - thus allowing her to float. The recovery operation was originally meant to take place 15 days after

her sinking (3rd August, 1545). The Admiralty was confident in the ships recovery as this was considered to be a relatively simple operation; the ship had sunk in shallow enough water that her masts still protruded above the surface. Additionally, the Venetian salvagers were considered experts in the field. By the 7th August, all that had been achieved was the recovery of the sails and yard arms, as well as the securing of the masts with cables. However, Charles Brandon reported to William Paget that the Mary Rose would be recovered "... this afternoon or tomorrow". Despite this, by August 9th it was reported that the operation had been delayed by the snapping of the Mary Rose's masts. On the 8th December, the Venetian salvagers were paid 40 Marks and informed that their services would no longer be required (Stirland, 2005) (Raising the Mary Rose, 2021).

In 1965, 'Project Solent Ships' was formed with the aim of investigating shipwrecks in the Solent via the use of dive teams and sonar. On the 5th of May 1971, divers discovered three port frames belonging to the Mary Rose. In 1978, after several dives onto the wreck, the decision was made to excavate the ship in its entirety. Finally, in 1982, the Mary Rose was raised. A purpose-built lifting frame was attached via wires to steel bolts passing through the hull. The steel frame was positioned above the wreck and hydraulic jacks were used to break the vacuum seal caused by the encasing silt. Once hanging from the frame, the wreck was transferred into a steel cradle which in turn was lifted by a crane attached to the vessel Tog Mor (Raising the Mary Rose, 2021).

Upon final excavation of the wreck, remains of ~45% of the crew were recovered. Bones from 179 individuals were found. Of these, 92 fairly complete skeletons (FCS) have been identified (Reconstructing the Crew of the Mary Rose, 2021). Due to the rapid nature of the sinking and environmental conditions in the Solent, the wreck became quickly encased in silt. It is thought that the 'first Tudor layer' of silt formed within months, however, the wreck was not thought to be fully encased in silt until the 3rd layer of sediment formed towards the end of the 16th and 17th centuries (Marsden, 2015). This rapid encasement resulted anaerobic conditions and therefore allowed for "excellent preservation of much organic material" including the FCSs. Because of is, analysis has been able to be performed on the remains. Recently, isotopic analysis performed on Mary Rose remains has found evidence pointing to the geographical

origin of the crew members being more diverse than previously thought (Scorrer et al., 2021).

1.2: Dual-Energy X-Ray Absorptiometry (DEXA)

Dual-energy X-ray absorptiometry (DEXA) is a non-invasive method for the measurement of soft tissue composition and bone mineral status of the skeleton (Bolotin et al., 2001) (Mazess et al., 1990).

In clinical settings, DEXA is typically used to aid in the diagnosis of osteoporosis (Radiology (ACR), 2022), however it can also be used as a method for determining body composition (Radiology (ACR), 2022).

DEXA utilises two X-ray beams with distinct energies. These are emitted from a radiation source below the subject and pass through the subject (Shepherd et al., 2017). These X-rays are attenuated differently by soft tissue and bone, and the level of attenuation of the two beams can be used to accurately calculate body composition, bone mineral content (BMC), and bone mineral density (BMD) (Griffiths, 1994) (Shepherd et al., 2017).

When used to aid in the diagnosis of osteoporosis, the calculated BMD values can be converted into values relating to averages across the population using the equations shown below (Berger, 2002).

$$\bullet T\ score\ = \frac{patient's\ BMD—population\ peak\ BMD}{standard\ deviation\ (SD)\ of\ population\ peak\ BMD}$$

$$\bullet Z\ score\ = \frac{patient's\ BMD—population\ age\ related\ BMD}{SD\ of\ population\ age-related\ BMD}$$

Figure 1.2.1. Equations used for the calculation of T and Z scores.

In adult women, osteoporosis is diagnosed if the T score is <-2.5 standard deviations from the average population (Kanis et al., 1994).

1.3: Bone Adaptation

Bone is a complex and highly organised tissue (Meyer et al., 2006). The formation of bone is a process consisting of numerous steps which can be characterised by interactions between various bony tissue cells, components of the extracellular matrix, and inorganic materials (Meyer et al., 2006) (Setiawati & Rahardjo, 2018).

A key factor in bone formation is biomechanical loading (Frost, 1994). A German anatomist and surgeon by the name of Julius Wolff theorized that bone adaptation would occur in response to the repeated loads under which it is placed (Frost, 1994). Wolff proposed that if the load under which a bone is placed increases, bone remodelling will occur to such an end that the bone will be better equipped to cope with the increased load (Frost, 1994). Furthermore, he hypothesized that if the load under which a bone was placed decreases, the bone's homeostatic mechanisms would shift toward a catabolic state (Frost, 1994).

It is now widely accepted that the remodelling of a bone in adaptation to load state of loading is facilitated via a mechanotransduction mechanism (Teichtahl et al., 2015). Mechanotransduction mechanisms are processes by which mechanical signals are converted to biochemical responses through cellular signalling. Mechanotransduction mechanisms can be broken down into the following steps: mechanocoupling, biochemical coupling, signal transmission, and cell response (Teichtahl et al., 2015).

1.4: Gelatin

Gelatin is a high molecular weight polypeptide derived from collagen (Poppe, 1992). Collagen is obtained by the partial hydrolysis of collagen derived from the skin, bones, and connective tissues of animals (typically cows and pigs) (Poppe, 1992). Gelatin's elastic mechanical properties mean it closely resembles human tissue (Anugrah et al., 2020).

Gelatin is commonly used as a soft tissue ballistic simulant (Fackler & Malinowski, 1985). The widely accepted method of mixing ballistic gelatin was developed by Fackler and Malinowski (Fackler & Malinowski, 1985). The solution is poured into moulds and allowed to set in the refrigerator for 24 hours.

Bloom refers to the scale used to measure the strength of gelatin (Bloom, 1925). The scale ranges from roughly 90 bloom (weakest) to roughly 300 (strongest) (Bloom,

1925). The test to measure bloom was developed in 1925 by Oscar T. Bloom. The test measures the weight (in grams) required by a plunger with a diameter of 0.5 inches to depress the surface of the gel 4mm without it breaking. In order to perform the test, the gelatin must be made to a concentration of 6.67% and kept at a temperature of 10°C prior to the start of the test. The number of grams applied by the plunger is the gelatin's bloom value (Bloom, 1925). Whilst the bloom value typically refers to the strength of a gelatin, it can also be used in reference to the gel's melting and gelling points – the higher the bloom value, the higher the gels melting and gelling points, and the shorter it's gelling times (Bloom, 1925).

Gelatins are typically categorised as "low", "medium", and "high". See *Table 1.4.1* for the typical values for these subranges (MM Ingredients, 2018).

Table 1.4.1. A table describing the different categories of gelatin bloom.

Category	**Bloom Number**	**Average Molecular Mass**
Low Bloom	50–125	20,000–25,000
Medium Bloom	175–225	40,000–50,000
High Bloom	225–325	50,000–100,000

1.5: DEXA with Historic Human Remains

While most commonly used for the determination of BMD within living samples (Morgan & Prater, 2017), there are existing studies that use DEXA as a method for determining the BMD of historic human remains (Navega et al., 2017). In order to simulate the soft tissue required to perform a DEXA scan, a soft tissue proxy (STP) must be used. The most commonly used STP in existing literature is a dry rice bed (Navega et al., 2017) (Borrè et al., 2015) (Hale & Ross, 2018) (Taylor et al., 2020). There are also published studies that use a water bath as an STP (Brødholt et al., 2021). Despite the aforementioned study's reporting the use of these STPs, there is little, if any, rationale stated for their use. Furthermore, the reporting, in terms of the reliability of these STPs, is equally sparse. If reported at all, method reliability data is cursory and void of detail.

1.6: Research Proposal

Whilst limited, evidence exists to support the theory that DEXA could be utilised as a non-invasive method for the measurement of BMD within historical samples. There is very little existing literature on the use of DEXA with archaeological remains and that which does exist gives minimal indication as to the optimal methodology for reliable and repeatable results. Furthermore, with the knowledge of bone adaptation to differing loads through Wolff's Law, if BMD data was able to be collected from a sample of Mary Rose remains, this could be used to gain insight into the possible occupations and physical activity levels of the sailors on board.

Therefore, the purpose of this study is:

Aims:

To measure bilateral asymmetry in a sample of paired radii from human remains collection of the Mary Rose Trust.

Objectives:

1) To develop a criterion method to measure BMD, using DEXA of historical human remains.
2) Use the criterion method to investigate bilateral asymmetry in a sample of historic human remains, specifically paired radii.

This study hypothesises that the criterion method for the use of DEXA on historical remains will require both the determination of an optimum STP, in terms of the material and volume of STP used, and the determination of an optimum sample preparation prior to scanning. Furthermore, this study hypothesises that once determined, the use of a criterion method to measure BMD bilaterally within a population of paired radii, from the Mary Rose trust's collection, will allow for measurement of significant differences in BMD between dominant and non-dominant radii due to principles of bone loading and adaption.

Chapter 2

Literature Review

2.1. Accuracy and Precision, Measurement Error, Reliability, and Validity

2.1.1. Accuracy and Precision

2.1.2. Measurement Error

2.1.3. Reliability

2.1.4. Validity

2.2. Bone Mineral Density (BMD)

2.3. Dual-Energy X-Ray Absorptiometry (DEXA) as an Instrument for Measuring Bone Mineral Density (BMD) in Historical Remains

2.3.1. Analysis of Historical Remains using DEXA

2.3.2. Review of Existing Literature

2. Literature Review

2.1. Accuracy and Precision, Measurement Error, Reliability, and Validity

2.1.1 Accuracy and Precision

Accuracy is commonly used interchangeably with precision and both terms are frequently used in the scientific literature to describe the quality of measurements or methods (Selvik & Abrahamsen, 2017) (Strauss et al., 2006). Traditional definitions of the terms differentiate the two terms through the association of 'accuracy' with systematic errors and 'precision' with random errors – however, multiple definitions of both terms exist, and their meaning may vary as such (Selvik & Abrahamsen, 2017) (Strauss et al., 2006). Strauss et al., (2006) defines accuracy as the conformance to a recognised standard, or as close to the true value, desired, or required result. They go on to define precision as the inner accuracy of measurements. Precision is determined by repeating an experiment many times under the same circumstances with a constant measuring device or system. Precision is not related to the repeatability of a measurement, but with the stability of the measurement device or its reading during the measurement process. Through these definitions, Strauss et al., (2006) concludes that accuracy is not the same as precision. Accuracy and precision can be represented through the analogy of archery targets. If an archer fires multiple arrows spread randomly across a target, the archer would be deemed to have low accuracy and low precision. A second archer fires multiple arrows, these arrows are grouped close tightly together but not near the bullseye. This archer would be deemed to have low accuracy but high precision. A third archer fires multiple arrows, these arrows all land near the bullseye but are grouped loosely. This archer would be deemed to have high accuracy but low precision. A fourth archer fires multiple arrows, these arrows are all grouped tightly around the bullseye. This archer would be deemed to have high accuracy and high precision.

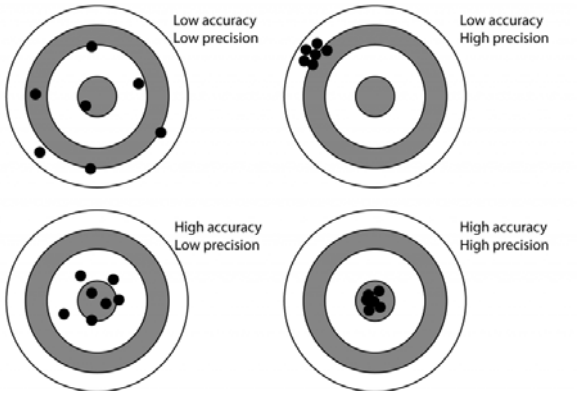

Figure 2.1.1.1. Visual demonstration of accuracy and precision

2.1.2. Measurement Error

Measurement error is the difference between the true value of a variable and the recorded value whilst measuring (Bland & Altman, 1996) (Glen, 2016). Measurement error consists of random error and systematic error. Random errors are naturally occurring errors that must be expected with any experiment. Systematic errors are errors brought on as a result of mis-calibrated equipment that will affect all measurements (Bland & Altman, 1996) (Glen, 2016). For example, when measuring the weight of subjects, if the scales were calibrated incorrectly by a magnitude of 1 N, then all measurements taken using that scale will be off by a degree of 1 N – this is systematic error. However, if the subjects were measured with differing levels of hydration between measurements, the deviation from the true value would be as a result of random error. Whilst measurement error is unavoidable, strong research design such as double-checking equipment calibration and proper training can aid in the reduction of these errors (Glen, 2016).

2.1.3. Reliability

Reliability refers to the consistency of a measurement (Heale & Twycross, 2015). When conducting a study, the values measured should be as similar as possible across repeated measurements (Heale & Twycross, 2015). It is not possible to accurately calculate reliability although it can be estimated based on three attributes: homogeneity, stability, and equivalence. Homogeneity (also known as internal consistency) refers to the extent to which all items on a scale measure a single

construct (Heale & Twycross, 2015). Homogeneity can be assessed using several tests: item-to-total correlation, split-half reliability, Kuder-Richardson coefficient, and Cronbach's α (Heale & Twycross, 2015). Stability refers to the consistency of results using an instrument with repeated testing (Heale & Twycross, 2015). Stability can be assessed using test-retest and parallel or alternate form reliability testing (Heale & Twycross, 2015). Equivalence refers to the consistency among responses of multiple users of an instrument, or among alternate forms of an instrument (Heale & Twycross, 2015). Equivalence can be assessed through inter-rater reliability (Heale & Twycross, 2015).

2.1.4. Validity

Validity refers to the extent to which a concept is measured accurately throughout a quantitative study (Heale & Twycross, 2015). For example, a study designed to measure the body weight of participants that measured solely the height of participants would not be considered valid. There are three major types of validity: content validity, construct validity, and criterion validity (Heale & Twycross, 2015). Content validity refers to the extent to which a research instrument accurately measures all aspects of a construct (Heale & Twycross, 2015). Construct validity refers to the extent to which research implements measures the intended construct (Heale & Twycross, 2015). Criterion validity refers to the extent to which a research instrument is related to other instruments that measure the same variables (Heale & Twycross, 2015). Validity is closely linked with reliability as they must both be considered when assessing the quality of a qualitative study (Heale & Twycross, 2015). An example of validity and reliability is a clock tower that rings at the same time each hour but not at the top of each hour. The clock is considered reliable as it rings at the same time each hour but not valid as it is meant to ring at the top of each hour. This shows the importance of considering both validity and reliability in research design.

2.2. Bone Mineral Density (BMD)

BMD can be described as the measure of inorganic material (primarily calcium and phosphorus) content in bone (Angelo, 2016) (Kranioti et al., 2019). BMD is considered one of the most informative bone quality assessments in both clinical and forensic settings, BMD values can provide a snapshot of bone health and can be used

for the identification of clinical conditions such as osteoporosis (NIH Osteoporosis and Related Bone Diseases National Resource Center, 2018) (Kranioti et al., 2019). BMD is affected by a variety of factors, including age, sex, disease, genetics, and lifestyle (Kranioti et al., 2019). Because of its composite nature, bone has many unique mechanical properties. The main components of bone are its organic matrix (consisting of mainly type I collagen), and its mineral matrix (hydroxyapatite crystal embedded in the collagen fibres). The mineral component of bone is primarily responsible for bone strength, whilst the organic component is responsible for bone toughness and its plastic deformation (Kranioti et al., 2019) (Currey, 2003) (Boivin et al., 2008). BMD values can be expressed in two different ways – both with their own units. Volumetric BMD (vBMD) is defined as the ratio of bone mineral content to bone size and is expressed in units of grams per cubic centimetre for example, 0.5 g/cm^3. Areal BMD (aBMD) is defined as the bone mineral content per unit area and is expressed as grams per squared centimetre for example, 0.5 g/cm^2. These two methods of expressing BMD differ as aBMD is dependent on bone size – equivalent BMD values in bones of different size would result in the same vBMD value but differing aBMD values. As a result of this, it is important to consider what value of BMD is being expressed when interpreting results. Whilst these two methods differ, studies have found a positive correlation between vBMD and aBMD (Ott et al., 1997) (Liu et al., 2018).

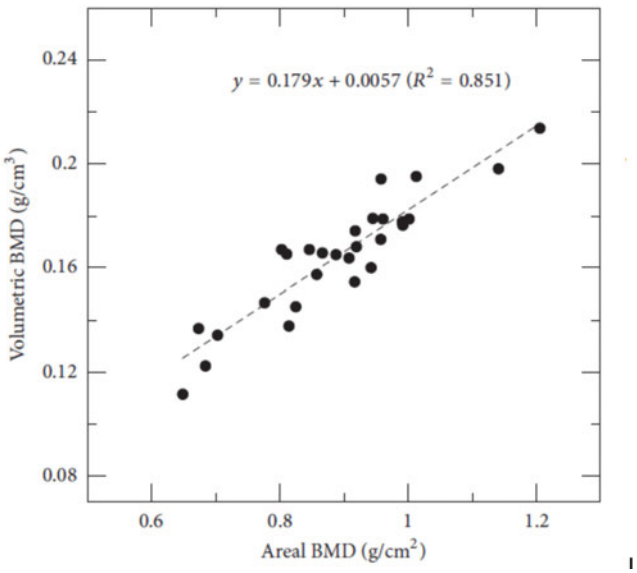

Figure 2.2.1. Correlation of vBMD and aBMD from study by Liu et al., 2018

In a clinical setting, BMD is primarily used to diagnose osteoporosis (EL Maghraoui & Roux, 2008). Osteoporosis is a systemic skeletal disease in which bone resorption exceeds bone formation and results in microarchitectural changes and leads to alterations in bone remodelling rates (Rachner et al., 2011). Bone remodelling is the process by which old and damaged bone is replaced with new bone. Bone remodelling consists of four phases: activation, where osteoclasts are recruited; resorption, where the osteoclasts resorb bone; reversal, where osteoclasts undergo apoptosis and osteoblasts are recruited; formation, where osteoblasts lay down new organic bone matrix that is subsequently mineralised (Frost, 1994) (Langdahl et al., 2016). Bone modelling is the process by which bones are shaped and reshaped by the action of independent osteoclasts and osteoblasts. The modelling of bone is responsible for the shaping of bones (Frost, 1994) (Langdahl et al., 2016). The alteration in bone remodelling can in turn lead to reduced bone strength and increased bone-fracture risk. Osteoporosis is most commonly diagnosed through BMD measurements of the lumbar spine and hip. BMD has also been used in forensic medicine and anthropology to estimate sex and age, identify pathological conditions, and assess diagenetic changes in bone material (Kranioti et al., 2019).

BMD can be measured in numerous ways. Diagnostic radiography/X-ray can be used to estimate BMD. X-rays can be used to visualise the morphology of bone but cannot provide a quantitative value of BMD (Kranioti et al., 2019). As such, the estimation of BMD is subjective and heavily influenced by user experience. As a result of this, X-rays are typically used as a screening tool to rule out factors that may affect bone-mass loss such as fractures (Kranioti et al., 2019). Despite this, literature does suggest that grayscale values from x-ray images are directly proportional to BMD and that there is good correlation between grayscale and BMD values (Macchiarelli & Bondioli, 1994).

Single photon absorptiometry (SPA) was introduced in 1963 by John Cameron and James Sorenson (Cameron & Sorenson, 1968). Through SPA it was possible to determine peripheral BMD by measuring the absorption of a monochromatic, low energy photon beam by the intended bone. This photon beam was generated by a radioactive source (most likely iodine-125 at 27.3 keV). In order to simulate soft

tissue in SPA, the region of interest (ROI) would be submerged in water. Cameron and Sorenson reported that SPA produced results that were accurate and reproducible to within ~3%. Despite the reported accuracy and repeatability of SPA, the method was limited in that the target region had to be surrounded by water and as such, only appendicular bones could be measured (Cameron et al., 1968).

In 1965, dual photon absorptiometry (DPA) was introduced (Mazess et al., 1981). The introduction of a dual energy source allowed for the measurement of the axial skeleton; these regions were not able to be measured using SPA as they cannot be easily surrounded by water. DPA utilises a Gadolinium-153 source with 2 photon energies at 44 and 100 keV. The radiation beams pass through and are absorbed by the ROI and are then detected by a sodium iodide detector. The detector then analyses the beams for distinct 44 and 100keV peaks. The higher energy peak is absorbed by both bone and soft tissue whilst the lower energy peak is only absorbed by soft tissue. Mazess et al. (1981) found DPA to be highly accurate when measuring total body BMD – error levels of 1-1.5% in normal adults, 2% in older women, and 2.5% in osteoporotic females were reported.

Quantitative computed tomography (QCT) is another method for BMD determination. QCT is primarily used to evaluate BMD values in the lumbar spine and hip. QCT implements a higher dosage of radiation in comparison to other BMD measurement methods, this leads to images with higher resolutions – allowing for improved discrimination of uncalcified tissues. However, fat free mass can cause quantification errors (Kranioti et al., 2019) (Manske et al., 2010). The high exposure levels of QCT can be reduced through the implementation of volumetric QCT (vQCT) (Kranioti et al., 2019). vQCT allows for increased precision, of 5-10% deviation from actual values (Kranioti et al., 2019). Peripheral QCT (pQCT) has been developed for low-radiation-dose analysis of regions such as the distal radius and ulna (Kranioti et al., 2019). A more recent development is biomechanical CT, this method employs finite-element analysis (FEA) models which are able to predict the mechanical properties of the structure and fracture risk (Keaveny, 2010). The main benefit of CT-based BMD measurement methods is its ability to isolate and measure trabecular bone – drastically reducing the noise encountered in x-ray analysis methods. Another benefit is the ability to identify artifacts created by degenerative joint disease (Li et al., 2014).

Magnetic resonance imaging (MRI) can be used to measure vBMD. MRI utilises powerful magnets and applies the principles of magnetisation to generate images (Hong et al., 2000). MRI is commonly used in the assessment of the musculoskeletal system and associated pathology (Hong et al., 2000). Due to its lack of ionisation radiation, bone is visualised as low-intensity spaces in high-density soft tissue. Through this process, several aspects of bone architecture can be quantified (vBMD, bone volume/total volume, trabecular number, trabecular thickness, and trabecular separation) (Kraiger et al., 2012) (Hong et al., 2000). Whilst MRI has the distinct advantage of its lack of exposure to ionising radiation, it is limited by the procedure's high cost and the difficulty in standardising image quality and quantification (Hong et al., 2000) (Kraiger et al., 2012).

Dual-energy x-ray absorptiometry (DEXA) is widely considered to be the gold standard in non-invasive techniques for the measurement of BMD quick scan time, as well as its low radiation dose (Morgan & Prater, 2017). DEXA was first introduced in 1987 by Hologic Inc. as a replacement for DPA (DXA: The Gold Standard, 2022). This transition was necessitated by DPA's resolution limits, degrading energy source, and long scan times of up to 40 minutes. The replacement of the Gadolinium-153 source (energy peaks of 44 and 100 keV) with X-rays (energy peaks of 70 and 140 keV) led to increased resolution and precision as well as decreased scan times of just 6 minutes (scan times of some regions would later be lowered to just 1-2 minutes through the implementation of fan or array beams) (Mazess et al., 1981) (Wahner et al., 1988). A study by Cohen and Rushton (1995) found the precision error of DEXA to be 1.1-4.5% depending on the ROI – this precision error was calculated by scanning the region five times without replacing the sample, the sample was placed under a 10cm rice bed. The error of duplicate scans in patients was calculated using *Equation 1*:

$$Precision\ Error(\%) = 100 \times \sqrt{\frac{SD^2}{n}}$$

Equation 1. Precision Error

Where SD is the standard deviation and n the number of patients (Cohen & Rushton, 1995), however it is not clear what data was used to determine the standard deviation. Whilst there are multiple different manufacturers of DEXA systems (with each

manufacturer often offering more than one model of system), the general procedure for the determination of BMD remains the same across them all. A radiation source is aimed at a radiation detector, the patient is placed on a bed in the path of the radiation beam. ROI is scanned by the movement of the scanning arm (containing the radiation detector) over the ROI, allowing for X-rays attenuation in the ROI to be measured. The dual energy nature of DEXA allows attenuation measurements of both soft tissue and bone to be measured. The differential attenuation of the two energies by the patient are used to estimate the bone mineral content and soft tissue composition. The attenuation of X-rays is dependent on the patient's mass and composition. Because of the dual-energy X-rays, only two components can be determined at any one time and as such, the patient's body must be considered a dual-component attenuator (bone mineral and soft tissue attenuate X-rays at differing levels). To measure soft tissue composition, measurements must be made in regions with no bone present. BMD is calculated by the DEXA computer via the comparison of the two x-ray energies. The initial attenuated beam energies, and the emerging attenuated beam energies are used to calculate ratios of mass attenuation coefficients at low and high energies for soft tissue and bone respectively. The attenuation properties of soft tissue have been calibrated via the use of the DEXA system's software and phantoms of known composition (and therefore, known levels of attenuation). The tissue is assumed to be bone if the ratio measured exceeds the known value for pure lean tissues. DEXA expresses values as bone mineral content (BMC) or aBMD. Areal density is calculated using *Equation 2*:

$$aBMD = \frac{BMC}{Area}$$

Equation 2. Areal Bone Mineral Density (aBMD)

Because the value for density is areal, the orientation of the patient is crucial for obtaining accurate measurements, (Cohen & Rushton, 1995). If the patient shifts from the desired position, the areal 'shadow' will be altered, resulting in a potentially erroneous aBMD value. To illustrate this, consider an object such as a cylinder, which can be scanned in transverse and longitudinal orientations. If scanned in different orientations, the area exposed to the scan will differ, resulting in different aBMD values, despite the vBMD of the cylinder remaining constant.

2.3. Dual-Energy X-Ray Absorptiometry (DEXA) as an Instrument for Measuring Bone Mineral Density (BMD) in Historical Remains

2.3.1. Analysis of Historical Remains using DEXA

DEXA is widely considered to be the gold standard for non-invasive methods of measuring BMD in living patients (Morgan & Prater, 2017), there is very limited research into its use on historical remains i.e. non-living samples. In part, the reason for the lack of research could be DEXA's limitations when used to scan a sample without the presence of soft tissue, namely human remains. DEXA scanners are software driven, which means that raw data produced by the X-Ray sources undergoes considerable manipulations before any images or data are produced (Morgan & Prater, 2017) (DXA: The Gold Standard, 2022) (Berger, 2002). Part of the DEXA scanning process requires both bone and soft tissue to be present, the lack of soft tissue in historical remains leads to no image being generated without 'fooling' the scanner via the use of a soft tissue proxy (STP) such as rice (Navega et al., 2017). The existing research is limited in its methodology – making the replication of methods near impossible.

The assessment of BMD in historical populations can yield important information. As with modern populations, BMD values of historic human remains can provide insight into the osteological health of these populations. Whilst unable to be used to draw concrete conclusions without supplementary data historical BMD values could be used to aid with the determination of potential dietary trends and activity levels. BMD values are unable to be used on their own in these determinations as there are a myriad of other factors that can influence BMD such as disease and fracture history (Suzuki et al., 2019)

DEXA provides a useful tool for the measurement of BMD within historical samples. In addition to being considered the gold standard in non-invasive BMD determination methods due to its quick scan time and high resolution – DEXA also has a low ionising radiation dose per scan. The low ionising radiation dose minimises the risk of damaging any organic material. Murray (2022) conservatively estimates that the minimum annual radiation dose required to cause damage to organic structures is 50 mSv/yr, although it is unclear how these figures have been determined. A DEXA scan delivers a dose of between 1 – 15 μSv depending on the scanning protocol used

(International Atomic Energy Agency (IAEA), 2017). Despite the clear benefits, DEXA is limited in its ability to scan historical remains due to the requirement of an STP and the lack of standardisation.

2.3.2. Review of Existing Literature

Navega, Coelho, Cunha, and Curate (2017) used a dry rice bed as an STP to scan historical remains. The primary aim of this study was to explore the association of BMD with age. The secondary aim of the study was to create an accurate method to estimate death in human remains based on BMD features. This study utilised a sample of 100 femora collected from females whose death age ranged from 21 to 95 years. If the femora displayed gross diagenetic alterations or evidence of significant pathological conditions, it was excluded from the study. To assess the effect of soil erosion, a sample of 48 femora were radiographed. The results of these scans showed the effect of soil erosion was null. The measurement of BMD was performed using a Hologic DEXA scanner (QDR 4500C Elite Densitometer, Hologic, Marlborough, Massachusetts) (Hologic QDR-4500C Elite—Bone Densitometer, 2015). The selected femora were placed on a low-density cardboard recipient, this recipient in turn was placed atop a 10 cm rice bed - although no detail or justification was given for the protocol other than a reference to a book chapter. The femora were positioned along the anteroposterior axis, with diaphysis parallel to the scanner's longitudinal axis. Once positioned, the femora were internally rotated ~35° - thus increasing reproducibility, in terms of relative spatial position. The scanner automatically identified several regions of interest (ROI) (femoral neck, trochanter, intertrochanteric region, Ward's area, and total hip). From these ROIs, bone area (cm2), cone mineral content (g) and BMD (g/cm2) were determined semi-automatically; if necessary, minor adjustments to the ROI could be made . This study reported three variables - BMD total, BMD Ward, and BMD Neck. To test the repeatability of this study's method, 30 femora were scanned twice, and relative technical error of the mean (rTEM) was calculated. This study reported an rTEM value of 0.86% which was reported as being "a very low value". The study concluded that whilst the DEXA values obtained using this methodology were both precise and reproducible, BMD values could be affected by taphonomic processes - especially within archaeological samples (Navega et al., 2017). Navega et al. described in detail both the STP and steps taken to prepare each sample for scanning. This relatively rich methodology

allows for accurate reproduction of their method used. Additionally, Navega et al. (2017) provided insight into the precision of their method via the calculation of rTEM, however, no comparisons were provided to the precision of other methodologies – thus making it hard to conclude whether the reported value of 0.86% was a good level of agreement.

A study by Borrè, Boano, Di Stefano, Castiglione, Ciccone, Isaia, Panattoni, and Faletti (2015) aimed to investigate whether population differences in osteoporosis observed today reflects modern lifestyle factors or whether the differences were also present in historic populations. BMD data was collected from skeletal remains excavated from burial grounds in North-West Italy. More than 700 skeletons of adults, adolescents and infants dating back to the 8th-13th and 17th centuries were excavated. In order to be deemed suitable for inclusion in this study, materials needed to be undamaged and void of signs of pathological features or signs of soil erosion/infiltration. Lumbar vertebral bodies (L1-4) and/or femurs from 27 male and 28 female adult individuals were selected for use in this study. This study reported the use of a fan-beam densitometer to DEXA scan the samples. Prior to scanning, the standardised positioning of samples was achieved by placing the samples in a padded box. The samples were positioned on the scanning bed in the frontal plane with the femurs being placed on the condyles and the greater trochanter. Simulation of soft tissue was achieved via the use of a dry rice bed. No further detail regarding sample positioning was given in the methodology, this method, as described by Borrè et al. (2015), is potentially prone to placement error. BMD averages were calculated for the lumbar spine and femoral neck using the DEXA scan outputs with linear regression models being used to estimate missing data for lumbar spine BMD (Borrè et al., 2015). Borrè et al. (2015) provided minimal detail with regard to the STP used in their methodology. They reported samples were placed in dry rice, but no detail was given as to the volume, depth, or type of rice used. Additionally, limited detail was given with regard to the preparation of samples other than they were placed in a padded box on their frontal plane with the aim of this being to standardise their position – as such, accurate replication of this method would be challenging. Furthermore, the study reported no values for repeated measures testing of a single, or multiple samples. No information as to the precision and repeatability of their method was reported making meaningful interpretation of the data problematic.

A study by Hale and Ross (2018) aimed “to introduce a promising, novel method to aid in the assessment of bone quality in forensically relevant skeletal remains”. This paper provides detailed methodology for the anatomical positioning and DEXA analysis of skeletal remains. This paper also presents three case studies which aim to illustrate the efficacy of DEXA in forensic scenarios. Hale and Ross (2018) outline three major steps in their bone scanning protocol: machine preparing, performing exam, and analysing exam. This protocol utilises a rice bed as an STP: a container was filled with rice; the sample was placed upon the rice bed and the exposed bone was covered with rice. Hale and Ross (2018) reported the results of a scan on the skeletal remains of a deceased, white, female, aged 31 years old. AP lumbar spine and left hip scans were performed on this individual and a total BMD score of 0.944 g/cm2 (t-score = -0.9). The first case study presented by Hale and Ross (2018) studied a 40-year-old male exhibiting a series of rare fractures on his tibial and femoral surfaces. Traditional fracture timing methodologies were inconclusive in determining whether the fractures were peri- or post-mortem. As such, to assess whether the acute fractures were a result of fracture fragility or merely a post-mortem artifact from natural drying processes. In order to obtain a BMD value, a left hip DEXA scan was obtained. The left hip was selected due to the presence of longitudinal fractures in the femora and tibiae as well as the incomplete nature of the lumbar spine. A total BMD value of 1.299 g/cm2 with a t-score of 1.8 was calculated from the DEXA scan. This result indicates that bone insufficiency was most likely not the cause of the longitudinal fractures. The second case study presented by Hale and Ross (2018) studied a 13-year-old female with a suspected history of long-term abuse. Numerous antemortem fractures consistent with childhood abuse were present in the remains. Current methodologies for the assessment of malnutrition include the comparison of long bone lengths to that of a reference sample. The limb lengths for this individual were 300 mm and 355 mm for the left femur and tibia respectively, these limb length values were matched, most closely to that of a 9-year-old. Ruff’s equation (Ruff et al., 2012) was used to estimate juvenile stature based on the femur and tibia lengths. The estimated stature was 136.2 cm. This value lies below the 3rd percentile when compared to the CDC 2000 growth curves for girls aged 2-20. BMD was assessed to provide insight as to the degree of malnutrition – the association between BMD loss and poor malnutrition is well established. The results an AP trabecular spine scan found a total BMD value of 0.660 g/cm2 and a corresponding z-score of -2.2. The

calculated z-score was consistent with low BMD for chronological age, thus providing more evidence for malnutrition. The third case study presented by Hale and Ross (2018) studied a 14-month-old infant whose suspected cause of death was starvation. The remains were still in the early stages of decomposition and had a mass of 6.1kg. Gomez et al. (1955), and Waterlow classification methods were used to estimate malnutrition. Gomez et al., (1955) classified the infant's weight at 38% when compared to that of the reference sample – equivalent to grade 3, severe malnutrition. The Waterlow system classifies 38% as severe wasting (Hale & Ross, 2018). Hale and Ross provided minimal detail as to the STP used and their sample preparation process – only stating that samples were placed in a container filled with rice and that exposed bone was then to be covered again with rice (the type of rice was not specified). These minimal details, make this methodology's accurate reproduction difficult to achieve. Furthermore, whilst rich BMD data was reported in this study, no values for repeated measures testing were reported, making accurate interpretation of this data difficult.

A study by Sutlovic, Boric, Sliskovic, Popovic, Knezovic, Nikolic, Vucinovic, and Vucinovic (2016) aimed to investigate the difference in BMD obtained via DEXA and the chemical determination of calcium and phosphorus concentrations in skeletal remains. This study utilised cortical bone samples taken from femoral remains exhumed from mass graves from the Second World War. Fragment samples (average length of 4.59 cm) were taken from equal positions from the right and left femur (under the minor trochanter on the upper femur). DEXA scans were performed on 72 samples (36 pairs). Scans were performed using the lumbar spine programme on a Hologic QDR 4500 C densitometer. A standard profile (Caucasian male, weight 75 kg, height 175 cm) was used. The study reported BMD values ranging from 1.245 g/cm2 – 1.789 g/cm2 (Sutlovic et al., 2016). This study does illustrate the ability of DEXA to be used to measure BMD within historical samples, it offers minimal detail as to the exact DEXA protocol used, especially with regard to the soft-tissue proxy or sample preparation used. As such the ability to reproduce this method is impossible. Furthermore, there are no values reported for repeated measures testing, as such, the precision and repeatability of the method cannot be assessed, therefore making accurate interpretation of this data difficult.

A study by Taylor, Hammer, Zwirner, Ondruschka, and Kieser (2020) aimed to investigate the validity of Bos taurus scapulae as a proxy for human frontal bones by comparing laminar and cancellous bone thickness, as well as the BMD of cadaveric frontal bones and adult Bos taurus scapulae. This study utilised 3 Bos taurus scapulae and 13 human frontal bones (8 male and 5 female). BMD was measured using a GE Lunar Prodigy densitometer. White rice was used as soft-tissue proxy. Samples were placed in a plastic container on top of the rice. Samples were then scanned using a full body scan protocol. An average BMD value was taken from an ROI (20 cm2) in size, the ROI was situated "just below the spine of the scapula", however no reason for this choice of ROI was stated. The study reported BMD values of 0.4±0.1 g/cm2 in the Bos taurus scapulae and 0.5±0.1 g/cm2 in the human frontal crania (Taylor et al., 2020). This study does comment on the STP and sample preparation used, Taylor et al. (2020) states that samples were placed atop a plastic container of rice. However, the methodology does not include details as to the volume of white rice used, or the positioning of samples within the rice bed – as such, the ability to replicate this method is limited. Additionally, there is no comment on repeated measures values, thus, the precision and repeatability of the method is unable to be established.

A study by Brødholt, Günther, Gautvik, Sjøvold, and Holck (2021) aimed to investigate the processes and factors that influence the development in Osteoporosis by analysing human remains. Brødholt et al. (2021) reported that research on archaeological skeletal material from Norway has focused mainly on the medieval period and lead to few conclusive results regarding long-term trends and patterns of changes from prehistoric to modern times. As such, this study aimed to address the gap in current literature. This study utilised remains from the Schreiner Collection at the Division of Anatomy, University of Oslo – this collection consists of ~8,500 skeletal finds. The final sample used for this study consisted of 316 (137 female, 179 male) sets of femoral remains. The samples were divided into groups depending on age and socioeconomic status. The following age groups were applied: young (20–35years old), middle (35–50 years), and old adult (50 +). The following socioeconomic groups were applied: high, mixed, parish population, and low (socioeconomic status was identified based on information from literature and (previous) osteological analyses). BMD values were obtained using a lunar iDXA scanner (Lunar iDXA, GE Healthcare, Chicago, Illinois). BMD was measured at the

region of interest defined at the femoral neck. Whilst this study acknowledges that a rice bed as the standard STP, this method is not recommended with the Lunar iDXA as the high-resolution images generated will portray the grains of rice (Brødholt et al., 2021). As such, this study used a combination of water and plastic boards as an STP. A specially constructed frame was used to allow the positioning of the sample between the plastic boards and the water container. The water level in the container was set to a level of 14.5 cm. The samples were positioned anterior surface up and angled in such a way that the femur neck lay horizontally, and the femur diaphysis was oriented parallel to the scanner's longitudinal axis. This study measured BMD at the femoral neck. This methodology was validated by scanning each femur three times in order to assess precision and repeatability. The Lunar iDXA manufacturer reports expected precision error for repeated measurement to be ≤1.0% (GE, 2014), the observed precision error of this study was 0.7% (Brødholt et al., 2021). Brødholt et al. provided a detailed methodology in terms of the STP, and sample preparation used – thus allowing for accurate replication of their method. Furthermore, Brødholt et al. reported low values of 0.7% precision error indicating good precision (this value is less than the expected 1.0% threshold reported by the manufacturer). Whilst the methodology reported allows for accurate replication and indicates high precision, there is no investigation into the application of alternate STPs or sample preparations.

Chapter 3

Methodology

3. Methodology

This study consisted of two main phases. Phase one consisted of developing a criterion method for the use of Dual-Energy X-ray Analysis (DEXA) as a method of measuring bone mineral density (BMD) within historic human remains. Phase two consisted of a bilateral analysis of left/right radii BMD within a population of historic human remains recovered from the Mary Rose wreck.

3.1. Materials

A sample of 20 pairs of radii bones from the Mary Rose Trust collection were used for this study. Each pair consisted of a left and right radius from the Trust's collection of 'fairly complete skeletons' (FCS).

Samples were stored in a secure, fire-proof cabinet inside a locked office. The samples were stored in ambient temperatures and out of direct sunlight to avoid damage. When scanned, the samples were transferred to a PELI Protector case (PELI, Manchester, United Kingdom) for transportation to the DEXA lab. Upon completion of scanning, the samples were transferred back to the PELI Protector case and transported back to the storage office. This transportation protocol minimised the risk of any damage occurring to the samples whilst in transit.

3.2. Method

3.2.1. General Scan Method

Samples were scanned using a Stratos DR densitometer (Stratos, DMS Imaging, Montpellier, France). Prior to scanning, it was ensured that the scanner was within the required temperature limits, this was done by switching the scanner on ~30 minutes before testing. When the scanner had reached the manufacturer's defined operating temperature, a quality control check was performed. A phantom, of known density, was placed on the scanner and scanned. The Stratos software automatically calculated whether the scanner was recording density within acceptable limits, and this was displayed, *Figure 3.2.1.1*.

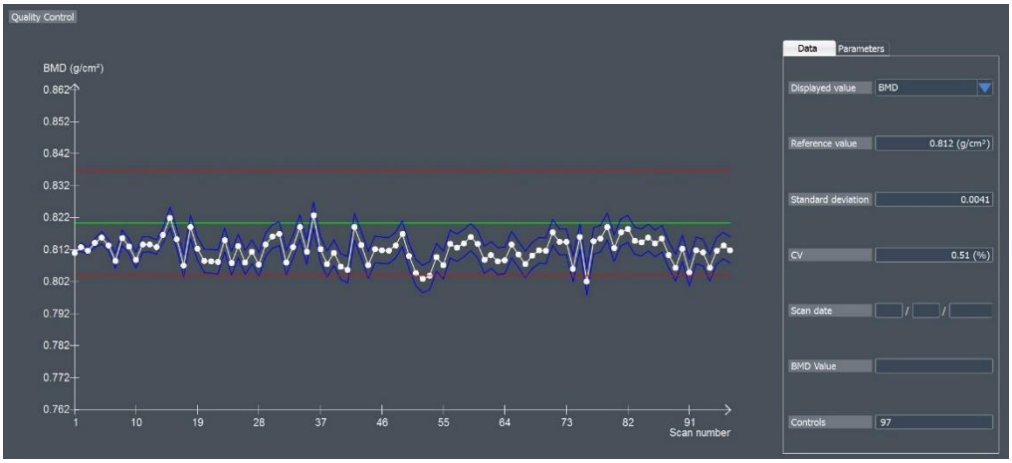

Figure 3.2.1.1. Quality control output. Screenshot taken from Stratos software.

After ensuring the scanner was performing within acceptable limits (defined as the red limit of agreement lines in *Figure 3.2.1.1*), the preparation of samples could commence. When prepared, the sample was placed on the DEXA Scanner's bed in either pronated or supinated position. When pronated, the sample would be positioned "palm down". When supinated, the sample would be positioned "palm up".

The Stratos DR software was then opened and the "Scan" option was selected. A patient profile was required for the Stratos software to allow a scan to occur. Each sample was given a patient ID according to the following template: FCS no. + Left/Right Radius + Pronated/Supinated. For example, FCS29RRPRO refers to the right radius of FCS29 being scanned in the pronated position. Every sample was given the same first name (Mary), last name (ROSE), birth date (01/01/2001), sex (Male), ethnic group (Caucasian), height (180cm), and weight (90kg), as shown in *Figure 3.2.1.2*. Once completed, the patient creation window was saved.

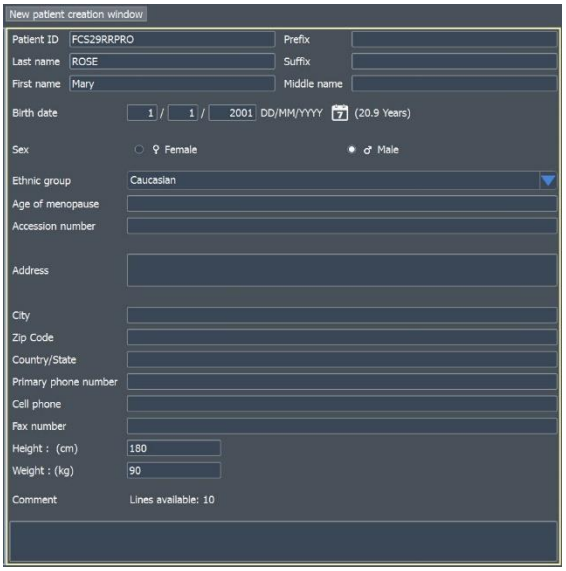

Figure 3.2.1.2. Patient creation window. Screenshot taken from Stratos software.

Scans were performed using the Left Femur Protocol under the normal exposure setting. Left Femur was selected as the there was no option withing the DEXA software to adjust beam intensity or scan time. As such, there was no ability to perform different trials of scan setting. Scanning protocols corresponded to the general position of different bones when a participant would lie on the scanner bed. Each bone location had specific machine setting in which the X-Ray intensity, exposure time etc., were optimised for that particular bone. For example, a femur would have higher beam intensity as there is more soft tissue and bone compared to a humerus. Several protocols were trialled and the one which was judged to produce the best image was used. The protocol used for scanning the sample radii was the femur protocol, this protocol was chosen as it produce a clearer resolution than the forearm protocol.

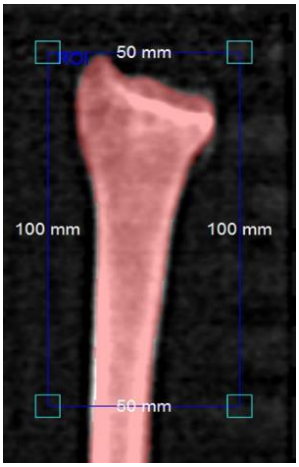

Figure 3.2.1.3. Left femur protocol. Screenshot taken from Stratos software.

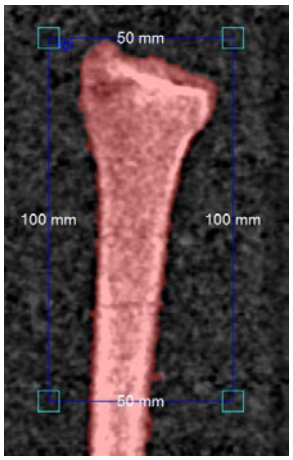

Figure 3.2.1.4. Forearm protocol. Screenshot taken from Stratos software.

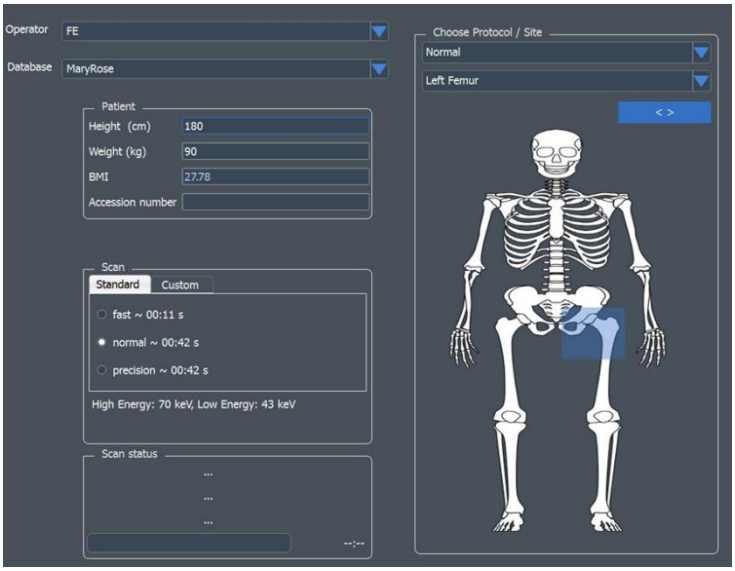

Figure 3.2.1.5. Pre-scan setting page. Screenshot taken from Stratos software.

Once the appropriate settings were selected, a scan was run. This caused the scanner arm to move to its initial position on the bed (whenever the scanning arm was in motion, all personnel present remained behind the black and yellow safety line). Once in position, the scanning arm projected a laser dot onto the bed, which acted as a reference point, allowing for precise positioning of the sample. Throughout the scan process, the image of the radius was monitored to ensure the positioning was correct. If not, the scan was aborted, and the "New Position" option was selected – allowing for repositioning through the Software before the scan was resumed and allowed to finish i.e., the physical position of the radius was not changed. Upon completion of the scan, the scan image is displayed. In the analysis screen, a custom region of interest (ROI) was drawn (as shown by the blue rectangle on *Figure 3.2.1.6*). The custom ROI was rectangular in shape with dimensions of 50 mm x 100 mm. This ROI was positioned at the most distal point of the image, *Figure 3.2.1.6*.

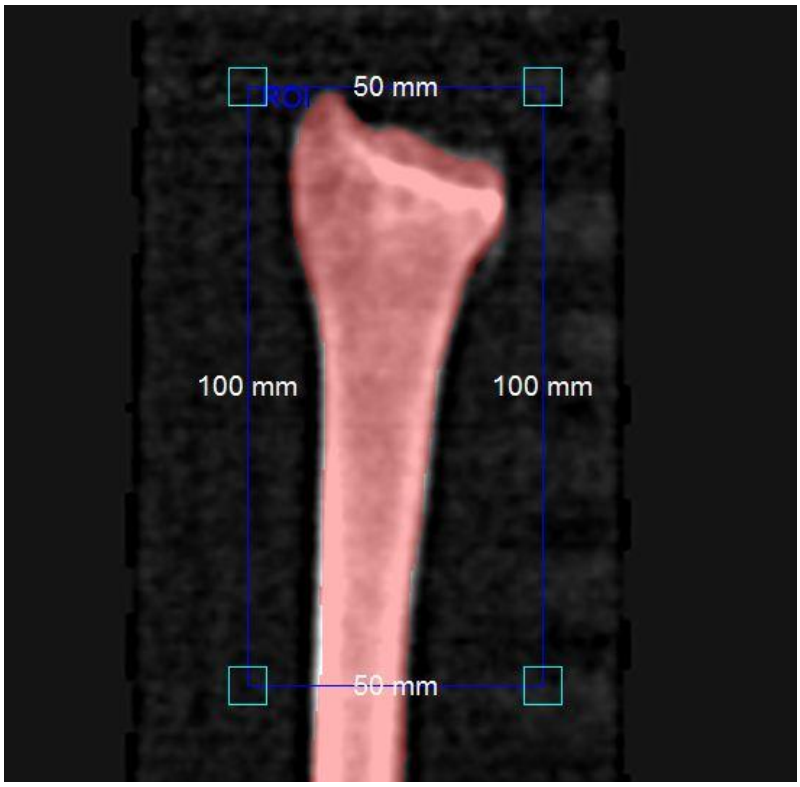

Figure 3.2.1.6. ROI positioning. Screenshot taken from Stratos software.

3.2.2. Phase 1: Development of a Criterion Method for the use of Dual-Energy X-Ray Absorptiometry (DEXA) on Historic Remains

In order to determine a criterion method for the use of DEXA on archaeological remains, the following phases were considered.

First, it was necessary to determine the optimal method of sample preparation in terms of the rice bed method and means of supporting the sample in a reliable position. Second, it was necessary to determine the most suitable soft tissue proxy (STP).

3.2.2.1. Determination of Optimum Sample Preparation

3.2.2.1.1. Rice Bed Method

To simulate soft tissue x -ray attenuation, an initial proxy consisting of a dry rice bed (Navega et al., 2017) (3cm depth) and two bags of rice flour (each weighing 900g). This depth of rice, and weight of rice flour was tested in a pilot study and found to produce the highest resolution scan image. The rice bed was contained within a plastic box. A plastic box was used to contain the STPs as the plastic would not attenuate the X-rays (Saps et al., 2014) and as such, would appear invisible on the scans.

The radius to be scanned was placed on the rice bed in the pronated or supinated position. Care was taken when placing the sample to minimise any potential disturbance of the rice bed. Once positioned, the bags of rice flour were placed, one at a time, over the distal head of each sample. It was vital that the placement of the bags of rice flour was done in such a way as to minimise any unwanted movement of the pre-positioned sample.

Once suitably positioned, the sample, in the rice bed, was placed on the DEXA scanning bed.

Upon the initiation of the scan, a red laser dot was projected onto the scanning bed to allow for accurate sample placement. The red dot was positioned on the radial shaft at the point immediately proximal to the rice flour bags, *Figure 3.2.2.1.1.1.*

Figure 3.2.2.1.1.1. Rice bed method - Sample positioning. A = laser reference point, B = dry rice bed, C = rice flour bags.

After positioning was completed, the scan. With ~10 seconds left on the scan; the scan was paused to allow for sample repositioning within the Stratos software. This was necessary due to the likelihood of the sample shifting within the rice bed after placement. The scan was then restarted with the new position and allowed to continue to completion, whereupon analysis of the scanned image could be conducted. Once the analysis of the scanned image was initiated, the software automatically calculated BMD.

3.2.2.1.2. Development of Suspension Bracket

The potential shifting of samples after their final positioning in the rice bed was potentially problematic beyond simple positioning errors. The DEXA scanner reported BMD values in g/cm2. This areal density value meant that the orientation along the longitudinal axis of the sample was important to be maintained. Any change in orientation would result in a different area "shadow" being scanned by the DEXA, this could potentially result in erroneous BMD values – especially when scanning the same sample multiple times.

To minimise the risk of the sample shifting when placed on the rice bed, a suspension bracket was developed to hold the sample in a known position – suspended between soft tissue proxies.

A prototype bracket was developed to test the efficacy and viability of this solution. The prototype consisted of a plastic box with a notch cut at one end to accommodate the proximal head of the sample. Two loops of bungee cord were wrapped around the box. The sample would be positioned in the pronated position (palm down) with the proximal head placed in the notch. One loop of cord would support the sample from the bottom, whilst the other was placed over the top of the sample – suspending the distal head of the sample. From this position, soft tissue proxies could be placed above and below the sample.

The final version of the suspension differed from the prototype in several aspects. Instead of cutting a notch into the box, a plastic support was mounted onto the box to

hold the proximal end of the sample. The support also had a plastic clamp that would support the sample's proximal shaft – negating the need for the bungee cords, *Figure 3.2.2.1.2.1*.

Figure 3.2.2.1.2.1. Final suspension bracket design

3.2.2.2. Determination of Optimum Soft Tissue Proxy (STP)

3.2.2.2.1. Gelatin Block Formation Method

To form the gelatin blocks, 240 bloom pork gelatin powder was used (MM Ingredients, Dorset, United Kingdom). Depending on the desired concentration of gelatin (a range of concentrations from 6-25% was used in this study), a specific amount of gelatin powder was weighed into a beaker and poured slowly into one litre of de-ionised water. Whilst being poured, the gelatin was stirred gently into the water until fully blended. The mixture was then placed into a fridge and allowed to bloom for two hours. After blooming, the mixture was removed from the fridge and heated slowly in a water bath until a temperature of 39˚C was reached. Throughout the heating process, the mixture was stirred slowly to achieve complete dissolution. Once fully dissolved, the gelatin mixture was poured into plastic moulds at a depth of 30mm. This depth was measured by taking a piece of metal with a known height of 30mm and placing it at the base of the mould, water was slowly poured into the mould until the depth matched the height of the metal piece. A line was then drawn

onto the mould, around the water level, thus giving an accurate guide for the required depth. Once poured, the moulds were placed in the fridge and allowed to set for a minimum of 24 hours.

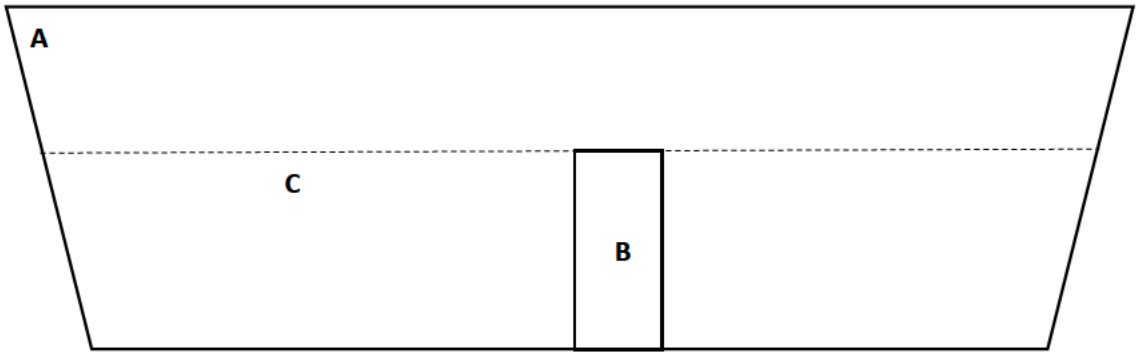

Figure 3.2.2.2.1.1. Diagram representing the method used to determine 30 mm gelatin blocks. A = plastic container, B = 30 mm metal guide, C = level of gelatin – calculated by drawing line at top of metal guide.

3.2.2.3. Optimal Sample Preparation Method & Soft Tissue Proxy (STP) Determination

To determine the optimal sample preparation method and STP, the reliability of each method and proxy had to be assessed. To achieve this, a radius was positioned on the scanner. The radius was then scanned 16 times without being disturbed or repositioned. From the collected data set, standard error of the mean could be calculated using *Equation 3*:

$$SEM = \frac{\sigma}{\sqrt{n}}$$

SEM = Standard error of the mean

σ = sample standard deviation

n = number of samples

Equation 3. Standard Error of the Mean

The value of standard error of the mean (SEM) was referred to as machine capability as it represents the error present in the DEXA scanner when no external variables such as sample positioning were changed. Whilst machine capability values provided a good representation of the DEXA scanner's error threshold with each method, it did not account for any errors that may arise when changing or repositioning samples –

the uncertainty associated with sample (radius) positioning was accounted for through the measurement of method capability. To determine method capability, a similar method was employed to that of machine capability determination. A sample was positioned on the scanner. This sample was then scanned 16 times, however, between each scan, the sample was removed from the scanner and repositioned. The aim of the repositioning was to simulate the disruption that would occur when changing the sample. When repositioning the sample, the operator aimed to replace the sample in as similar position as possible as they would when changing the sample. When the 16 scans were completed, *Equation 3* was used to determine the SEM.

Initially, this method was used to test the efficacy, in terms of reliability, of the suspension bracket when compared to the rice bed method. For the purposes of this test, rice was used as STP for both the suspension bracket and rice bed. After determining the efficacy of the suspension bracket, this sample positioning method was used to test for the optimal STP.

The suspension bracket was tested with both a rice bed proxy and 10% gelatin block proxy. A 10% gelatin proxy was used initially as this is the concentration used by the FBI to simulate soft tissue in ballistics testing (Fackler & Malinowski, 1985). After determining the viability of gelatin blocks as a STP, the optimal concentration of gelatin needed to be tested. Whilst the FBI uses a 10% solution for ballistics testing, this concentration is mixed with 250A bloom gelatin powder, as such, the actual optimal concentration may differ depending on the specific gelatin powder used (Fackler & Malinowski, 1985). This study used gelatin of bloom 240, in order to determine the concentration of 240 bloom gelatin that resulted in the optimum STP, a range of 6-25% gelatin was tested.

3.2.3. Phase 2: Reliability and Bi-lateral Asymmetry Analysis Using the Criterion Method

To determine bi-lateral asymmetry between left/right radial pairs within the samples, gelatin blocks (11.7% concentration) were used as an STP in conjunction with the suspension bracket method (the criterion method).

Each sample was scanned in 2 orientations – pronated and supinated. This was done as BMD is reported as an areal value by the DEXA scanner. As a result of this, the BMD value of each sample could vary depending on the orientation in which it was

scanned as the areal cross-section would be different. Scanning each sample in 2 orientations allowed for an average value to be taken of BMD and therefore gain a more accurate value for BMD. Each sample was scanned twice in each orientation, thus allowing for an average to be calculated and any anomalous values to be identified.

After scanning, the sample was weighed using a precision balance (Kern and Sohn PLJ 2000-3A, Kern, Balingen, Germany). The sample was then transferred back to the Peli Protection Case.

This process was repeated for the left and right radius of each FCS.

As the DEXA scanner was not intended for use on historical remains, the units generated were arbitrary due to the lack of data on chemical composition of the samples when compared to living tissue. Despite this, each sample was exposed to similar conditions when preserved in the layer of silt. As a result of this the values reported were proportional and as such could be compared within the population. However, due to the arbitrary nature of the values, the units of BMD were recorded as mass/cm^2 as opposed g/cm^2 as reported by the Stratos software.

3.3 Statistical Analysis

All quantitative data was initially recorded by hand on paper. These results were subsequently transferred to Microsoft Excel (Microsoft Corp. Version 16. Redmond, WA) for collation and processing. Data processing and analysis was performed using Microsoft Excel and IBM SPSS Statistics 28 (IBM Corp, 2019). Descriptive statistics for values from all samples were presented as following: mean ± SD. Percentage difference between two datasets was calculated using *Equation 4*:

$$Percentage\ Difference = \frac{|V1 - V2|}{[\frac{(V1 + V2)}{2}]} \times 100$$

V1 = Value 1

V2= Value 2

Equation 4. Percentage Difference

Normality within datasets was assessed using the Shapiro-Wilks test for normality. Shapiro-Wilks was used as it is deemed more appropriate for tests whereby the sample size <50 samples (Mishra et al., 2019). All data tested was found to follow normal distribution and as such only parametric tests were required (*Appendix A*). Independent t-tests were conducted to assess for statistically significant differences within populations (*Appendix B*) (*Appendix C*) (*Appendix D*). One-sided *p* values were used to assess significance as our hypothesis expected one population to be greater than that of the other (Ludbrook, 2013).

Agreement (reliability) was assessed using Bland and Altman (B&A) limits of agreement (Bland and Altman, 1986). Limits of agreement (1.96 x SD) and systematic bias were reported a B&A plot. Data for the agreement analysis were the same data for the bi-lateral comparison, Section 3.2.3.

Chapter 4

Results

4.1. Development of a Criterion Method for the use of Dual-Energy X-Ray Absorptiometry (DEXA) on Historic Remains

4.2 Reliability and Bi-lateral Analysis for Asymmetry of Left/Right Radius Bone Mineral Density (BMD)

Chapter 4. Results

4.1. Development of a Criterion Method for the use of Dual-Energy X-Ray Absorptiometry (DEXA) on Historic Remains

Table 4.1.1. Table describing repeated measures scans of Fairly Complete Skeleton (FCS) 8 right radius. Sample was scanned using rice bed method and with the suspension bracket (utilising the rice bed as a soft tissue proxy (STP)). Samples were scanned without adjustment between scans. The standard deviation (SD) of the 16 measurements is referred to as machine capability.

	Bone Mineral Density (mass/cm^2)	
Scan No.	Rice Bed Method	Suspension Bracket w/ Rice Bed STP
1	0.787	0.787
2	0.786	0.787
3	0.784	0.788
4	0.800	0.786
5	0.797	0.776
6	0.797	0.783
7	0.789	0.785
8	0.790	0.781
9	0.796	0.783
10	0.801	0.784
11	0.799	0.787
12	0.798	0.778
13	0.797	0.783
14	0.799	0.786
15	0.800	0.776
16	0.801	0.782
Mean	0.795	0.783
SD	0.0058	0.0039
SEM	0.0015	0.00096

The first stage was to determine the reliability of measuring bone mineral density (BMD) with a fixed sample, to determine machine capability *Figure 4.1.1*. As shown, the sample was scanned 16 times, without adjustment between scans. The suspension bracket method reported a standard deviation (SD) = 0.0019 mass/cm^2 lower than that of the rice bed method (0.0039 and 0.0058 mass/cm^2 respectively). From these values, standard error of the mean (SEM) was calculated. The suspension bracket reported a

mean ± SEM of 0.783±0.00096 mass/cm^2 (±0.12%). The rice bed reported a mean ± SEM of 0.795±0.0015 mass/cm^2 (±0.19%).

Table 4.1.2. Table describing repeated measures scans of FCS 8 right radius. Sample was scanned using rice bed method and with the suspension bracket (utilising the rice bed as a soft tissue proxy (STP)). Samples were scanned with removal and repositioning of the radius between scans – sample was removed and replaced between each scan. Referred to as method capability.

	Bone Mineral Density (mass/cm^2)	
Scan No.	Rice Bed Method	Suspension Bracket w/ Rice Bed STP
1	0.794	0.798
2	0.787	0.799
3	0.795	0.800
4	0.782	0.805
5	0.787	0.806
6	0.788	0.804
7	0.794	0.806
8	0.788	0.809
9	0.786	0.806
10	0.781	0.802
11	0.793	0.809
12	0.795	0.804
13	0.775	0.807
14	0.802	0.807
15	0.803	0.804
16	0.795	0.808
Mean	0.790	0.805
SD	0.0075	0.0034
SEM	0.0019	0.00085

The second stage was to determine the reliability of measuring BMD with a removed and replaced sample, to determine method capability *Figure 4.1.2.* As shown, the sample was scanned 16 times, between scans the sample was removed from the rice bed or suspension bracket and placed back in – simulating the use of each method with a full sample population. The suspension bracket reported a SD 0.00410 mass/cm^2 lower than that of the rice bed method (0.0034 and 0.0075 mass/cm^2 respectively). From these values, standard error of the mean was calculated. The

suspension bracket reported a mean ± SEM of 0.805±0.00085 mass/cm^2 (±0.11%). The rice bed provided a mean ± SEM of 0.790±0.0019 mass/cm^2 (±0.24%).

Table 4.1.3. Repeated scans of FCS 8 right radius. Sample was scanned using suspension bracket to aid with sample positioning with gelatin blocks as soft tissue proxy (STP). Five concentrations were initially tested (6%, 8%, 10%, 15%, and 25%). Samples were not adjusted between scans.

	Bone Mineral Density (mass/cm^2)				
Scan No.	6% Gelatin Blocks	8% Gelatin Blocks	10% Gelatin Blocks	15% Gelatin Blocks	25% Gelatin Blocks
1	0.773	0.756	0.763	0.726	0.742
2	0.766	0.752	0.763	0.726	0.750
3	0.767	0.755	0.763	0.746	0.745
4	0.760	0.758	0.762	0.725	0.749
5	0.758	0.766	0.765	0.739	0.753
6	0.762	0.754	0.764	0.739	0.756
7	0.754	0.764	0.767	0.723	0.764
8	0.763	0.765	0.760	0.732	0.757
9	0.757	0.763	0.766	0.733	0.759
10	0.754	0.758	0.764	0.736	0.758
11	0.761	0.765	0.764	0.731	0.737
12	0.754	0.759	0.764	0.724	0.748
13	0.757	0.768	0.763	0.733	0.757
14	0.751	0.762	0.764	0.735	0.766
15	0.749	0.764	0.762	0.729	0.742
16	0.756	0.766	0.763	0.735	0.755
Mean	0.759	0.761	0.764	0.732	0.752
SD	0.0063	0.0050	0.0016	0.0064	0.0082
SEM	0.0016	0.0012	0.00041	0.0016	0.0020

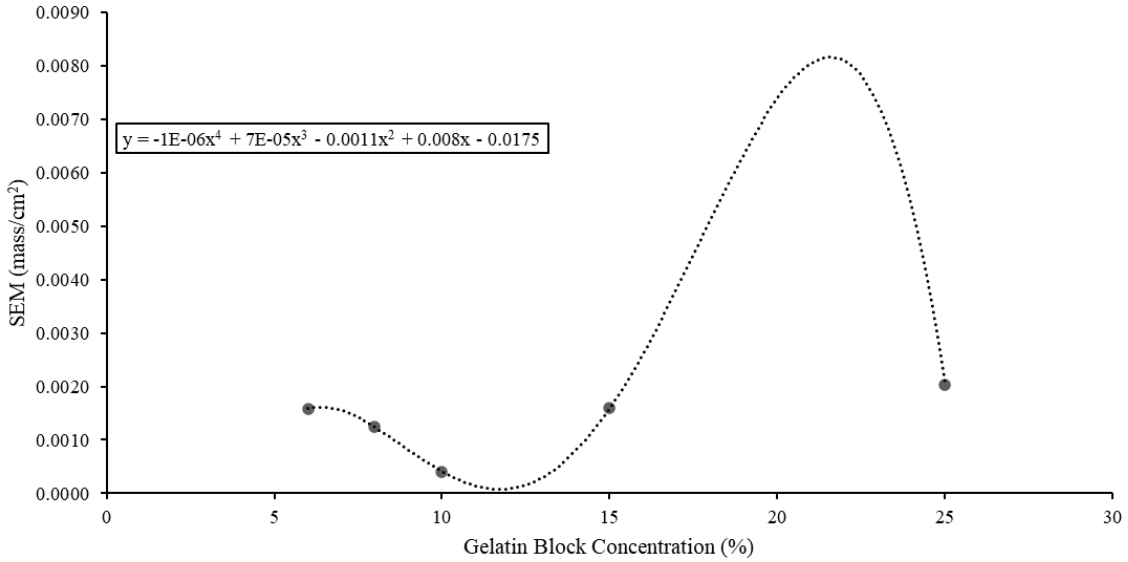

Figure 4.1.1. Line chart representing standard error of the mean (SEM), plotted against gelatin block concentration.

The first phase in determining the efficacy, in terms of reliability, of gelatin blocks as an appropriate STP, *Table 4.1.3*. The sample was scanned 16 times, without movement between scans. Initially, five concentrations of gelatin were assessed (6%, 8%, 10%, 15%, and 25%). The 10% gelatin blocks reported the lowest SD (0.0016 mass/cm^2) when compared with the other concentrations. The 25% gelatin blocks reported the highest SD (0.0082 mass/cm^2). From these values, SEM was calculated. The 6% gelatin blocks reported a mean ± SEM of 0.759±0.0016 mass/cm^2 (±0.21%). The 8% gelatin blocks reported a mean ± SEM of 0.761±0.0012 mass/cm^2 (±0.16%). The 10% gelatin blocks reported a mean ± SEM of 0.764±0.00041 mass/cm^2 (±0.054%). The 15% gelatin blocks reported a mean ± SEM of 0.732±0.0016 mass/cm^2 (±0.22%). The 25% gelatin blocks reported a mean ± SEM of 0.751±0.0020 mass/cm^2 (±0.27%).

The SEM values plotted on a chart with gelatin block concentration % along the x-axis and SEM along the y-axis is shown in *Figure 4.1.1*. A 4th degree polynomial trendline was drawn with the following equation:

$$y = -1E-06x^4 + 7E-05x^3 - 0.0011x^2 + 0.008x - 0.0175$$

From this trendline a lowest SEM could be estimated at 11.7% gelatin.

Table 4.1.4. Table describing repeated measures scans of FCS 8 right radius. Sample was scanned using suspension bracket and gelatin blocks as soft tissue proxy (STP). Six concentrations were tested (8%, 9%, 10%, 11%, 11.7%, and 13%). Samples were not adjusted between scans.

	Bone Mineral Density (mass/cm^2)					
Scan No.	Suspension Bracket w/ 8% Gelatin Blocks	Suspension Bracket w/ 9% Gelatin Blocks	Suspension Bracket w/ 10% Gelatin Blocks	Suspension Bracket w/ 11% Gelatin Blocks	Suspension Bracket w/ 11.7% Gelatin Blocks	Suspension Bracket w/ 13% Gelatin Blocks
1	0.785	0.701	0.684	0.680	0.751	0.695
2	0.783	0.699	0.684	0.683	0.751	0.697
3	0.781	0.701	0.684	0.681	0.751	0.695
4	0.789	0.705	0.682	0.681	0.750	0.702
5	0.788	0.704	0.683	0.681	0.750	0.698
6	0.780	0.695	0.684	0.685	0.752	0.698
7	0.778	0.704	0.683	0.683	0.750	0.702
8	0.788	0.699	0.685	0.683	0.754	0.698
9	0.783	0.703	0.686	0.681	0.751	0.698
10	0.790	0.702	0.683	0.684	0.753	0.697
11	0.780	0.703	0.683	0.682	0.751	0.699
12	0.783	0.702	0.682	0.682	0.751	0.699
13	0.782	0.705	0.688	0.682	0.751	0.697
14	0.787	0.703	0.686	0.685	0.751	0.702
15	0.781	0.707	0.684	0.682	0.752	0.689
16	0.784	0.701	0.682	0.681	0.750	0.705
Mean	0.784	0.702	0.684	0.682	0.751	0.698
SD	0.0036	0.0029	0.0017	0.0015	0.0011	0.0037
SEM	0.00090	0.00072	0.00041	0.00037	0.00028	0.00091

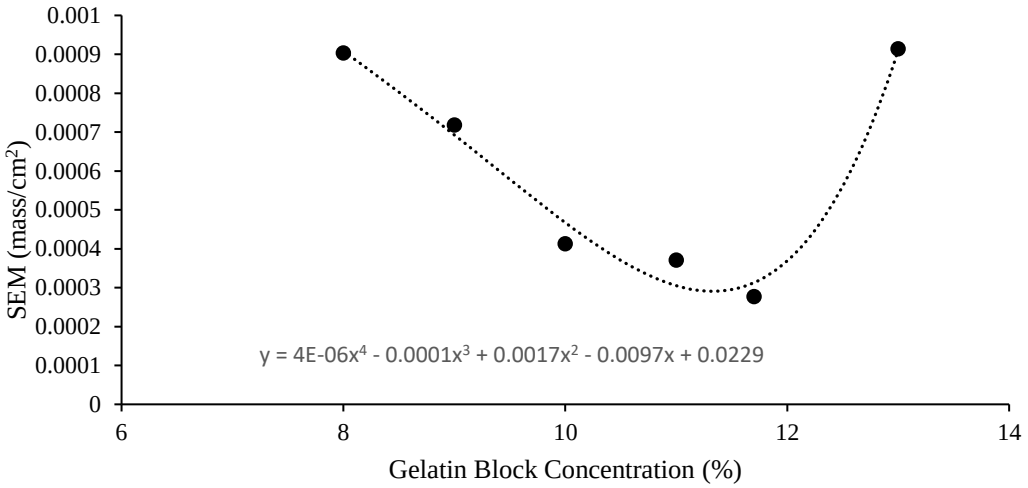

Figure 4.1.2. Line chart representing standard error of the mean (SEM), plotted against gelatin block concentration.

The second phase of ascertaining the efficacy, in terms of reliability, of gelatin blocks as an appropriate STP is shown in *Table 4.1.4*. The purpose of this second stage was twofold: to test a narrower range of gelatin block concentrations, and to assess whether the machine service performed on the DEXA scanner had impacted the scanner's exposure levels. In this stage, six concentrations of gelatin were assessed (8%, 9%, 10%, 11%, 11.7%, and 13%). The 11.7% gelatin blocks produced the lowest SD (0.0011 mass/cm^2). The 13% gelatin blocks reported the highest SD (0.0037 mass/cm^2). From these values, SEM calculated. The 8% gelatin blocks reported a mean ± SEM of 0.784±0.00090 mass/cm^2 (±0.11%). The 9% gelatin blocks reported a mean ± SEM of 0.702±0.00072 mass/cm^2 (±0.10%). The 10% gelatin blocks reported a mean ± SEM of 0.684±0.00041 mass/cm^2 ± (0.060%). The 11% gelatin blocks reported a mean ± SEM of 0.682±0.00037 mass/cm^2 ± (±0.054%). The 11.7% gelatin blocks reported a mean ± SEM of 0.751±0.00028 mass/cm2 (±0.037%). The 13% gelatin blocks reported a mean ± SEM of 0.698±0.00091 mass/cm^2 (±0.13%).

SEM values plotted on a chart with gelatin block concentration % along the x-axis and SEM along the y-axis are expressed in *Figure 4.1.2*. A 4th degree polynomial trendline was drawn with the following equation:

$$y = 4E - 06x4 - 0.0001x3 + 0.0017x2 - 0.0097x + 0.0229$$

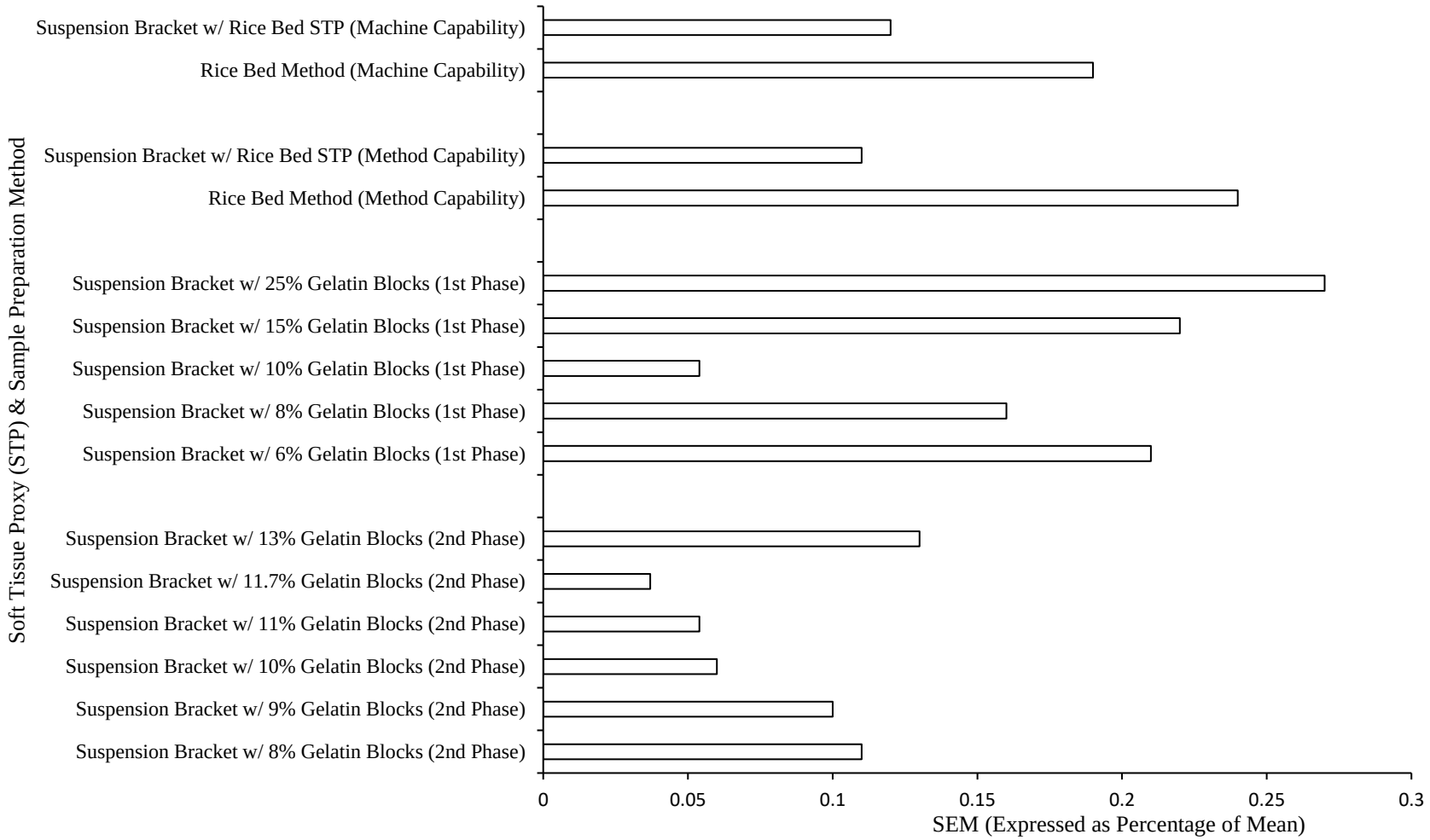

Figure 4.1.3. Bar chart representing standard error of the mean (SEM) values of all repeated measures tests.

4.2 Reliability and Bi-lateral Analysis for Asymmetry of Left/Right Radius BMD

Table 4.2.1. Full scan data for radius BMD. Samples were scanned using suspension bracket with 11.7% gelatin blocks as soft tissue proxy (STP) (Criterion Method)

Fairly Complete Skeleton (FCS) Bone ID	Right Radius (RR) / Left Radius (LR)	Mass (g)	Pronated Orientation (PRO) / Supinated Orientation (SUP)	Bone Mineral Density (BMD) (mass/cm^2)		
				Scan 1	Scan 2	Mean
FCS8	RR	59.55	PRO	0.751	0.751	0.751
			SUP	0.749	0.749	0.749
	LR	57.06	PRO	0.768	0.768	0.768
			SUP	0.762	0.763	0.763
FCS9	RR	43.19	PRO	0.562	0.563	0.563
			SUP	0.551	0.552	0.552
	LR	40.66	PRO	0.579	0.579	0.579
			SUP	0.561	0.561	0.561
FCS28	RR	47.87	PRO	0.642	0.643	0.643
			SUP	0.628	0.625	0.627
	LR	52.23	PRO	0.694	0.696	0.695
			SUP	0.670	0.670	0.670
FCS30	RR	51.18	PRO	0.710	0.710	0.710
			SUP	0.710	0.710	0.710
	LR	47.07	PRO	0.689	0.688	0.689
			SUP	0.685	0.686	0.686
FCS37	RR	57.29	PRO	0.746	0.745	0.746
			SUP	0.743	0.742	0.743
	LR	57.62	PRO	0.738	0.739	0.739
			SUP	0.732	0.732	0.732
FCS42	RR	55.38	PRO	0.762	0.762	0.762
			SUP	0.759	0.758	0.759
	LR	55.34	PRO	0.750	0.751	0.751
			SUP	0.746	0.746	0.746
FCS46	RR	51.17	PRO	0.711	0.712	0.712
			SUP	0.722	0.721	0.722
	LR	51.26	PRO	0.787	0.788	0.788
			SUP	0.768	0.767	0.768
FCS48	RR	52.77	PRO	0.645	0.644	0.645
			SUP	0.613	0.611	0.612
	LR	51.8	PRO	0.628	0.627	0.628
			SUP	0.600	0.605	0.603
FCS54	RR	48.12	PRO	0.568	0.568	0.568
			SUP	0.563	0.562	0.563
	LR	48.31	PRO	0.605	0.604	0.605
			SUP	0.602	0.602	0.602
FCS80	RR	59.16	PRO	0.663	0.663	0.663
			SUP	0.656	0.655	0.656
	LR	60.06	PRO	0.702	0.697	0.700
			SUP	0.693	0.694	0.694
FCS82 *	RR	54.26	PRO	1.448	1.449	1.449

			SUP	1.441	1.441	1.441
	LR	66.5	PRO	1.753	1.748	1.751
			SUP	1.745	1.743	1.744
FCS89	RR	49.82	PRO	0.703	0.703	0.703
			SUP	0.688	0.687	0.688
	LR	51.97	PRO	0.697	0.696	0.697
			SUP	0.671	0.671	0.671
FCS90	RR	52.93	PRO	0.774	0.775	0.775
			SUP	0.774	0.775	0.775
	LR	52.63	PRO	0.763	0.760	0.762
			SUP	0.757	0.755	0.756
FCS14	RR	64.1	PRO	0.824	0.825	0.825
			SUP	0.820	0.818	0.819
	LR	57.72	PRO	0.708	0.708	0.708
			SUP	0.675	0.675	0.675
FCS79	RR	52.42	PRO	0.685	0.686	0.686
			SUP	0.672	0.671	0.672
	LR	50.61	PRO	0.653	0.650	0.652
			SUP	0.646	0.646	0.646
FCS29	RR	55.31	PRO	0.721	0.721	0.721
			SUP	0.704	0.704	0.704
	LR	54.06	PRO	0.710	0.711	0.711
			SUP	0.700	0.701	0.701
FCS85*	RR	59.19	PRO	1.122	1.121	1.122
			SUP	1.072	1.072	1.072
	LR	62.14	PRO	1.050	1.049	1.050
			SUP	1.024	1.026	1.025
FCS84	RR	39.64	PRO	0.603	0.603	0.603
			SUP	0.598	0.599	0.599
	LR	41.4	PRO	0.778	0.777	0.778
			SUP	0.773	0.773	0.773
FCS7	RR	58.43	PRO	0.711	0.710	0.711
			SUP	0.712	0.713	0.713
	LR	56.89	PRO	0.711	0.712	0.712
			SUP	0.687	0.687	0.687
FCS75	RR	50.26	PRO	0.623	0.623	0.623
			SUP	0.603	0.603	0.603
	LR	53.71	PRO	0.980	0.980	0.980
			SUP	0.965	0.965	0.965

*Indicates FCS with observable discolouring – indicating that samples had been contaminated whilst on seabed. Because of this observation, the highlighted samples are removed from any data manipulation.

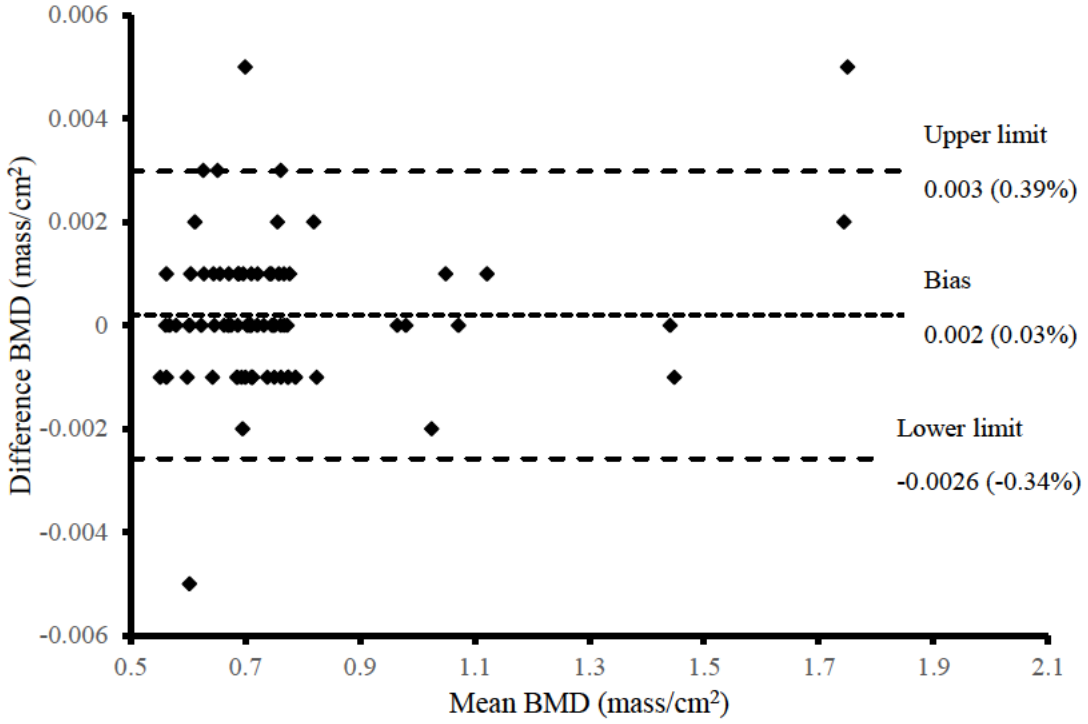

Figure 4.2.1. Bland and Altman limit of agreement plot for test, re-test data. Radii were scanned twice, scan 1 and scan 2, (Table 4.2.1).

Table 4.2.2. Table describing percentage difference in bone mineral density (BMD) between dominant and non-dominant radii for combined BMD values.

Fairly Complete Skeleton (FCS) Bone ID	Bone Mineral Density (BMD) (mass/cm^2)									
	Dominant				Non-Dominant			Pronated Percentage Difference (%)	Supinated Percentage Difference (%)	Combined Percentage Difference (%)
	Pronated	Supinated	Combined	Left/Right Radius Dominant?	Pronated	Supinated	Combined			
FCS8	0.768	0.763	0.766	Left	0.751	0.749	0.750	2.24	1.85	2.05
FCS9	0.579	0.561	0.570	Left	0.563	0.552	0.558	2.80	1.62	2.22
FCS28	0.695	0.670	0.683	Left	0.643	0.627	0.635	7.77	6.63	7.21
FCS30	0.710	0.710	0.710	Right	0.689	0.686	0.688	3.00	3.44	3.22
FCS37	0.746	0.743	0.745	Right	0.739	0.732	0.736	0.94	1.49	1.22
FCS42	0.762	0.759	0.761	Right	0.751	0.746	0.749	1.45	1.73	1.59
FCS46	0.788	0.768	0.778	Left	0.712	0.722	0.717	10.13	6.17	8.16
FCS48	0.645	0.612	0.629	Right	0.628	0.603	0.616	2.67	1.48	2.09
FCS54	0.605	0.602	0.604	Left	0.568	0.563	0.566	6.31	6.70	6.50
FCS80	0.700	0.694	0.697	Left	0.663	0.656	0.660	5.43	5.63	5.53
FCS82*	1.751	1.744	1.748	Left	1.449	1.441	1.445	18.88	19.03	18.95
FCS89	0.703	0.688	0.696	Right	0.697	0.671	0.684	0.86	2.50	1.67
FCS90	0.775	0.775	0.775	Right	0.762	0.756	0.759	1.69	2.48	2.09
FCS14	0.825	0.819	0.822	Right	0.708	0.675	0.692	15.26	19.28	17.25
FCS79	0.686	0.672	0.679	Right	0.652	0.646	0.649	5.08	3.95	4.52
FCS29	0.721	0.704	0.713	Right	0.711	0.701	0.706	1.40	0.43	0.92
FCS85*	1.122	1.072	1.097	Right	1.050	1.025	1.038	6.63	4.48	5.58
FCS84	0.778	0.773	0.776	Left	0.603	0.599	0.601	25.34	25.36	25.35
FCS79	0.711	0.713	0.712	Right	0.712	0.687	0.700	-0.14	3.71	1.77
FCS75	0.980	0.965	0.973	Left	0.623	0.603	0.613	44.54	46.17	45.35

*Indicates FCS with observable discolouring – indicating that samples had been contaminated whilst on seabed. Because of this observation, the highlighted samples are removed from any data manipulation.

Full scan results for all fairly complete skeleton (FCS) radius samples are shown in *Table 4.2.1*. Samples were scanned using the suspension bracket sample preparation method. 11.7% gelatin blocks were used as a STP. Samples were scanned in two orientations: pronated and supinated. The mean BMD value for pronated samples was 0.704 ± 0.0803 mass/cm^2. The mean BMD value for supinated samples was 0.693 ± 0.08234 mass/cm^2. From this, we can ascertain that on average, pronated BMD scans observed values 0.011 mass/cm^2 (1.587%) higher than supinated BMD values.

Values for percentage difference between dominant and non-dominant arm BMD values are shown in *Table 4.2.2*. On average, dominant arm pronated BMD values were 7.705 ± 11.321% greater than non-dominant arm values. Dominant arm supinated BMD values were 7.599 ± 11.155% greater than non-dominant arm values. Dominant arm combined BMD values were 7.182 ± 11.566% greater than non-dominant arm values.

When assessed for normality using the Shapiro-Wilk test. Dominant-Pronated, Dominant-Supinated, Dominant-Combined, Non-Dominant-Pronated, Non-Dominant-Supinated, and Non-Dominant-Combined datasets were all found to be normal ($p > 0.05$) ($p = 0.140$, $p = 0.282$, $p = 0.191$, $p = 0.306$, $p = 0.470$, and $p = 441$ respectively) (*Appendix A*).An independent t-test showed that a statistically significant difference exists between dominant and non-dominant pronated BMD values ($p < 0.05$, $p = 0.018$) (*Appendix B*). A statistically significant difference also exists between dominant and non-dominant supinated BMD values ($p < 0.05$, $p = 0.019$) (*Appendix C*). A statistically significant difference also exists between dominant and non-dominant combined BMD values ($p < 0.05$, $p = 0.018$) (*Appendix D*).

Chapter 5

Discussion

5.1. Development of a Criterion Method for the use of Dual-Energy X-Ray Absorptiometry (DEXA) on Historic Remains

5.1.1. Determination of Optimum Sample Preparation

5.1.2 Determination of Optimum Soft Tissue Proxy (STP)

5.2. Reliability and Bi-lateral Analysis for Asymmetry of Left/Right Radius Bone Mineral Density (BMD)

5.3. Considerations for Future Research

5.4. Conclusion

Chapter 5. Discussion

5.1. Development of a Criterion Method for the use of Dual-Energy X-Ray Absorptiometry (DEXA) on Historic Remains

5.1.1. Determination of Optimum Sample Preparation

Sample preparation was a vital stage in use of dual-energy X-Ray absorptiometry (DEXA) on historic remains. Sample preparation includes the orientation, around the longitudinal axis (LA), of the sample on the scanning bed as well as how the sample is placed with respect to the soft tissue proxy (STP). Inadequate sample preparation can lead to inaccurate and unreliable values of bone mineral density (BMD), this can be demonstrated by the lower standard deviation (SD) observed when samples were positioned using the suspension bracket compared to a rice bed (0.0039 mass/cm^2 and 0.0058 mass/cm^2 respectively). Due to the areal nature of the density values reported by DEXA (g/cm^2), the orientation in which the sample is placed is vital in producing accurate, precise, and repeatable results. With a non-uniform sample such as a radius, if the sample orientation is off by even a small factor, the BMD values calculated by the DEXA will vary, thus affecting reliability. This can be visualised by imagining a light shining from directly above the sample, we can take the shadow cast by the sample and use it to calculate the area used in the areal BMD value. However, if the sample is rotated around its LA, the shadow cast will subsequently change, and as such, so will the area used in areal BMD. As a result of this rotation, the value for BMD reported by the DEXA has changed, despite there being no change in the samples actual BMD value. As such, it is clear that sample preparation is a vital stage in achieving accurate, precise, and repeatable BMD values. This is in contrast to measuring BMD in a living participant as the participants bones will always be held in the same orientation as patients will be asked to lie on the scanner in a consistent, reference position.

The rice bed method was a poor method of sample preparation, as it produced more variable results - 0.795±0.0015 mass/cm^2 (±0.19%) compared to 0.751±0.00028 mass/cm^2 (±0.037%) (criterion method). Due to the malleable nature of the rice bed, it was hard to position the sample in a position that was accurately reproducible. Additionally, there was no guarantee that the sample would not shift from its desired orientation between its final placement and the onset of scanning – especially when

the 500g rice flour bags were placed on top of the sample. In order to minimise the risk of the sample shifting from its desired orientation, a bracket was developed to suspend the sample between the STP. By clamping the sample at the proximal shaft, the sample was unable to rotate, and as such, once positioned, we could be sure that the sample would not change orientation. Additionally, by suspending the sample between the STP, it was visible at all times, allowing visual confirmation that no alteration to its LA orientation had occurred – adding another layer of assurance.

In order to test the efficacy, in terms of reliability, of the suspension bracket, two rounds of testing had to be conducted. Initially, machine capability was tested in order to ascertain whether the suspension bracket allowed for accurate and precise DEXA scanning. Machine capability was tested by scanning a single sample sixteen times (using dry rice and rice flour as an STP) without adjustment between scans. The suspension bracket provided a standard error of the mean (SEM) of 0.00096 g/cm2. This value was 0.00054 g/cm^2 lower than when compared with the rice bed (SEM of 0.0015 g/cm^2). From it was established that the use of a suspension bracket in sample preparation allows for more accurate and precise DEXA scanning than the rice bed method of sample preparation. Once the machine capability of the suspension bracket was established, method capability needed to be tested. In many ways, this was a more important test as it determined the sample preparations practical efficacy by scanning a sample 16 times and removing and replacing the sample between each scan (again with dry rice and rice flour as an STP) – thus simulating the changing of samples that would occur when scanning multiple samples. In essence, this was testing the suspension bracket's ability to reproduce the same sample orientation with multiple samples. When tested for method capability, the suspension bracket measured a SEM of 0.00085 g/cm^2. This value was 0.0011 g/cm^2 than the value measured through the rice bed (SEM of 0.0019 g/cm2). Additionally, the suspension brackets values for method capability were in fact lower than its values for machine capability (-0.00011 g/cm^2 and – 0.011%) – this indicates that there is minimal difference in the suspension bracket's precision when removing and replacing the sample between scans than when the sample is left between scans. These values indicate the suspension bracket's ability to produce accurate, precise, and reliable results.

5.1.2 Determination of Optimum Soft Tissue Proxy (STP)

The choice of STP is important when using DEXA to scan historical remains. The nature of historical remains means that they only possess bone and not soft tissue. As such a proxy is required to simulate the presence of soft tissue and allow for a DEXA image to be captured – thus allowing BMD to be calculated. While rice has traditionally been used as a STP when using DEXA to scan historic remains, this study investigated the efficacy of gelatin as a potential STP.

Gelatin comprises of collagen and is derived from the electrolysis of animal skin, bones, and connective tissues. The elastic mechanical properties of gelatin mean it closely resembles human tissues in terms of physical properties and chemical composition. As such, it was reasonable to assume that gelatin would make a good proxy for human soft tissue with regards to its attenuation of X-rays and thus would make an appropriate STP.

In order to determine the efficacy of gelatin as an STP, the optimum concentration of gelatin needed to be assessed. Initially, machine capability was tested with five different concentrations of gelatin (6%, 8%, 10%, 15%, 25%). The logic behind this choice of concentration range was to establish an upper and lower bound of concentrations based around the assumption that the optimum concentration would be in the region of 10%. 10% was assumed to be the optimum as it is the established concentration used by the FBI to simulate human tissue (Fackler & Malinowski, 1985). From this initial range, the 10% gelatin blocks produced the lowest SEM (0.00041 g/cm^2). A 4th degree polynomial trendline was fitted on the SEM data from this range which indicated that the lowest SEM would be found at a concentration of 11.7% (*Figure 4.1.1)*. Based on this data, a second range of concentrations was tested with concentrations at 8%, 9%, 10%, 11%, 11.7%, and 13%. Some concentrations were re-tested as between the testing of the two ranges, the DEXA scanner underwent a servicing, and the exposure level was adjusted – by re-testing concentrations we were able to establish that the change in exposure had no effect on the SEM (*Appendix E*). From this second range, the 11.7% gelatin blocks reported the lowest SEM (0.00028 g/cm2). A 4th degree polynomial trendline was drawn based on the SEM data from this range, the SEM value for the 11.7% concentration fell below the

lowest point on this trendline (*Figure 4.1.2)* – indicating 11.7% as the optimum gelatin concentration for use as an STP.

5.2. Reliability and Bi-lateral Analysis for Asymmetry of Left/Right Radius Bone Mineral Density (BMD)

Reliability (agreement between test and re-test) was assessed using Bland and Altman limits of agreement (LOA) analysis which produced a sample mean = 0.762 mass/cm2, a systematic bias = 0.002 mass/cm2 (0.03%), upper LOA = 0.003 mass/cm2 (0.39%) and lower LOA = -0.0026 mass/cm2 (-0.34%). No existing studies reported reliability values for the method used to measure BMD in historic human remains using DEXA.

There was a statistically significant, difference in BMD between the dominant and non-dominant arms of our historical radius samples (*Appendix B*) (*Appendix C*) (*Appendix D*). Dominant arm was assumed to be the arm the higher BMD. We can assume that a subject's dominant arm will have experienced more mechanical loading over the subject's lifespan. According to Wolff's Law, we were able to assume that a subject's dominant arm will have a higher BMD due to having been placed under more mechanical load when compared to the non-dominant arm (Frost, 1994). However, through this assumption, we cannot take arm dominance to equal 'handedness'. This is because some activities that sailors aboard the Mary Rose would have undertaken (such as archery) traditionally rely on eye dominance to determine which arm is dominant (Mohammadi et al., 2016).

As a statistically significant difference was observed in all three BMD datasets (pronated: $p = 0.018$, supinated: $p = 0.019$, combined: $p = 0.018$) (*Appendix B*) (*Appendix C*) (*Appendix D*), we can assume that the sailors aboard the Mary Rose would favour the use of their dominant arm for the majority of load-bearing activities they were required to perform.

Furthermore, if we look on a more individual basis. Samples such as fairly complete skeleton (FCS)84 and FCS75 experienced far larger disparities between dominant and non-dominant BMD when compared to the average. FCS84 reported a 25.34% difference in pronated BMD (17.64% higher than average), a 25.36% difference in supinated BMD (17.77% higher than average), and a 25.35% difference in combined BMD (18.17% higher than average). FCS75 reported a 44.54% difference in pronated

BMD (36.83% higher than average), a 46.17% difference in supinated BMD (38.57% higher than average), and a 45.35% difference in combined BMD (38.17% higher than average). These larger than average disparities indicate that the sailors to whom these radius samples belonged would have potentially been in specialist careers that required repetitive, one-sided loading of the forearm. One possible explanation for this, is that the samples belonged to archers aboard the Mary Rose. The draw weight of a typical yew longbow could have been in the region of 150 pounds (Hemmings, 2019). Additionally, Tudor archers were considered elite soldiers and would likely have been trained from a young age (Wertman, 2015). The heavy draw weight and likely repetitive use of longbows would in theory lead to increased, asymmetrical bone loading patterns and as such could explain the large bilateral asymmetry in BMD observed in samples like FCS84 and FCS75.

In contrast to the large bilateral asymmetry in BMD observed in samples such as FCS84 and FCS75, several samples demonstrated minimal percentage BMD difference. For example, FCS79 reported a -0.14% difference in pronated BMD (7.85% lower than average), a 3.71% difference in supinated BMD (3.89% lower than average), and a 1.77% difference in combined BMD (5.41% lower than average). The minimal disparity between dominant and non-dominant arm BMD suggests that the sailors to whom theses samples belonged would have been tasked with activities that would not have resulted in frequent one-sided loading in their forearms. One possible explanation for this is that the samples belonged to a standard member of the crew. These sailors would be tasked with the operation of one of the ships cannons. These guns would have weighed up to 2 tonnes and were operated via the heaving and hauling of ropes (Stirland & Waldron, 1997). These activities, plus the requirements of moving the gun in general, would involve the use of both arms in a relatively equal manner. This could have resulted in more symmetrical bone loading patterns and as such would explain the minimal BMD disparity observed in samples like FCS 79.

5.3. Considerations for Future Research

Whilst the drawing of a custom region of interest (ROI) on the scan image allowed for us to be certain that BMD was being measured over the same area across all scans, it only provided an average BMD value calculated over the entire ROI – thus, not allowing for the determination of which areas in the distal radius head contained a

higher BMD than others. The software used to analyse scans has a function that allows for a colour gradient to be applied to the scan image – showing the differing BMD values across different regions of the radius (see *figure 5.3.1*). If standardised across all scans, this colour gradient could be used to assess which regions across the sample had higher BMD values and therefore, in theory, had undergone higher levels of bone loading. This data could be used to further aid in the determination of specific activities performed by the sailors to whom the samples belonged.

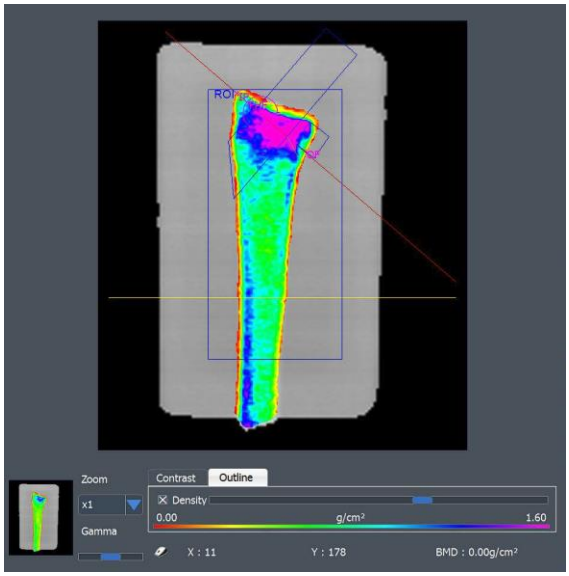

Figure 5.3.1. A scan output showing the BMD colour gradient applied to the left radius of FCS75.

Whilst each sample was scanned in two orientations (pronated and supinated) in order for an average (combined) BMD value to be calculated, there were observable differences between the pronated and supinated values. In order to provide a more comprehensive value for combined BMD, adjustments could be made to the suspension bracket – allowing for each sample to be rotated to known degrees. By measuring each sample in more orientations than merely pronated and supinated it would mitigate the risk of abnormally shaped radii from returning anomalous BMD values due to a non-uniform area being used to calculate areal BMD.

One limitation of this study was the assumption of arm dominance. Very limited records exist with regards to the final voyage of the Mary Rose. By far the most detailed record is the Anthony Roll (The British Library, 2023). The Anthony Roll is a record of the ships making up the Tudor navy in the 1540s. Named after its author, Anthony Anthony, the roll contains information pertaining to the size, crew,

armament, and basic equipment of each ship in King Henry VIIIs navy. Whilst the Anthony Roll provides vast detail into the cargo of the Mary Rose, no detailed information on the crew i.e. hand dominance was recorded (The British Library, 2023). The use of scientific laws such as Wolff's Law (Frost, 1994) allows informed assumptions to be made regarding arm dominance, however, these assumptions by no means can be taken as certainties. As a result of this, the conclusions drawn by this study based off these informed assumptions may be inaccurate.

Future research could build on the bi-lateral analysis performed in this study. One potential avenue for this is the comparison of dominant/non-dominant arm BMD disparity from the Mary Rose samples to modern day populations. For example, forearm DEXA scans could be performed on modern day archers – and the percentage BMD difference between dominant and non-dominant arm calculated. These values could be compared to the percentage BMD difference observed in Mary Rose samples – potentially providing more evidence as to the occupations of individual sailors.

5.4. Conclusion

This study consisted of two phases: the development of a criterion method for the use of DEXA on historic remains, which was then used to assess the reliability of the criterion method and the bi-lateral analysis for asymmetry of left/right radius BMD. This study reported a precision error of 0.145% (calculated using the same equation reported in Cohen & Rushton, 1995, *Equation 1*) when repeated measures testing (sixteen repeated scans without adjustment) was performed using the rice bed method of sample preparation. Additionally, a study by Cohen & Rushton (1995) testing the precision error of a 10cm rice bed reported a precision error of 1.1-4.5% when performing repeated measures testing (five repeated scans without adjustment between scans). The suspension bracket combined with 11.7% gelatin blocks reported a precision error of 0.028% (again, calculated using the same equation reported in Cohen & Rushton, 1995, *Equation 1*) when repeated measures testing (sixteen repeated scans without adjustment between scans) was performed. . The reliability of the criterion method, as assessed with B&A limits of agreement analysis produce excellent results (systematic bias= 0.03%, upper LOA = 0.39%, lower LOA = -0.34%). From this, it can be concluded that the implementation of a suspension bracket to aid with sample preparation prior to scanning as well as the use

of gelatin blocks (11.7% concentration) as a soft-tissue proxy led to the observation of more accurate, precise, and repeatable results when exposed to repeated measures testing, this is when compared to a traditional rice bed method. Consequently, it is recommended that in future when human remains are scanned, using a DEXA scanner, to determine relative BMD a suspension bracket is used to support the sample and gelatin blocks of 11.7% concertation are used.

Furthermore, this study found that statistically significant differences exist between dominant and non-dominant arm BMD. Additionally, the magnitude of these BMD values, when looked at on an individual scale, can be used to aid in hypothesising whether sailors were involved in occupations which required repetitive, asymmetrical bone loading – such as longbow archers, or occupations that would have required more balance, symmetrical levels of bone loading – such as general crew.

It was hypothesised that to produce a criterion method, the determination of optimum STP (both STP material and volume) and sample preparation was necessary. It was clear from the discussion in the previous paragraph that both needed to be carefully specified. Similarly, the second hypothesis stated that significant differences between dominant and non-dominant radii BMD would be measured when paired samples were scanned using the criterion method. When measurements were collected – significant differences were measured, thus affirming the second hypothesis.

Appendix

Appendix

Appendix A:

Tests of Normality

	Kolmogorov-Smirnov[a]			Shapiro-Wilk		
	Statistic	df	Sig.	Statistic	df	Sig.
CombDominant	.174	18	.157	.930	18	.191
CombNonDominant	.138	18	.200*	.951	18	.441
ProDominant	.153	18	.200*	.922	18	.140
ProNonDominant	.140	18	.200*	.941	18	.306
SupDominant	.167	18	.199	.939	18	.282
SupNonDominant	.113	18	.200*	.953	18	.470

*. This is a lower bound of the true significance.

a. Lilliefors Significance Correction

Appendix B:

Independent Samples Test

		Levene's Test for Equality of Variances		t-test for Equality of Means							
						Significance				95% Confidence Interval of the Difference	
		F	Sig.	t	df	One-Sided p	Two-Sided p	Mean Difference	Std. Error Difference	Lower	Upper
ProBMD	Equal variances assumed	.459	.503	2.189	34	.018	.036	.055667	.025432	.003982	.107351
	Equal variances not assumed			2.189	30.375	.018	.036	.055667	.025432	.003754	.107579

Appendix C:

Independent Samples Test

		Levene's Test for Equality of Variances		t-test for Equality of Means							
						Significance				95% Confidence Interval of the Difference	
		F	Sig.	t	df	One-Sided p	Two-Sided p	Mean Difference	Std. Error Difference	Lower	Upper
SupBMD	Equal variances assumed	.652	.425	2.164	34	.019	.038	.056500	.026115	.003429	.109571
	Equal variances not assumed			2.164	30.518	.019	.038	.056500	.026115	.003205	.109795

Appendix D:

Independent Samples Test

		Levene's Test for Equality of Variances		t-test for Equality of Means							
						Significance				95% Confidence Interval of the Difference	
		F	Sig.	t	df	One-Sided p	Two-Sided p	Mean Difference	Std. Error Difference	Lower	Upper
BMD	Equal variances assumed	.561	.459	2.182	34	.018	.036	.056111	.025718	.003845	.108377
	Equal variances not assumed			2.182	30.397	.018	.037	.056111	.025718	.003616	.108606

Appendix E:

Gelatin Concentration (%)	Pre-Service Standard Error of the mean (g/cm2)	Post-Service Standard Error of the mean (g/cm2)
8	0.0012	0.00090
10	0.00041	0.00041

Bibliography

Angelo, G. (2016). Bone Health In Depth. Linus Pauling Institute. https://lpi.oregonstate.edu/mic/health-disease/bone-health

Anugrah, M. A., Suryani, S., Ilyas, S., Mutmainna, I., Fahri, A. N., Jusmawang, & Tahir, D. (2020). Composite gelatin/Rhizophora SPP particleboards/PVA for soft tissue phantom applications. Radiation Physics and Chemistry, 173, 108878. https://doi.org/10.1016/j.radphyschem.2020.108878

Bell, L. S., Lee Thorp, J. A., & Elkerton, A. (2009). The sinking of the Mary Rose warship: A medieval mystery solved? Journal of Archaeological Science, 36(1), 166–173. https://doi.org/10.1016/j.jas.2008.08.006

Berger, A. (2002). Bone mineral density scans. BMJ : British Medical Journal, 325(7362), 484.

Bland, J. M., & Altman, D. (1986). Statistical methods for assessing agreement between two methods of clinical measurement. The lancet, 327(8476), 307-310.

Bland, J. M., & Altman, D. G. (1996). Measurement Error. BMJ : British Medical Journal, 312(7047), 1654.

Bloom, O. T. (1925). Machine for testing jelly strength of glues, gelatins, and the like (United States Patent No. US1540979A). https://patents.google.com/patent/US1540979/en

Boivin, G., Bala, Y., Doublier, A., Farlay, D., Ste-Marie, L. G., Meunier, P. J., & Delmas, P. D. (2008). The role of mineralization and organic matrix in the microhardness of bone tissue from controls and osteoporotic patients. Bone, 43(3), 532–538. https://doi.org/10.1016/j.bone.2008.05.024

Bolotin, H. H., Sievänen, H., Grashuis, J. L., Kuiper, J. W., & Järvinen, T. L. N. (2001). Inaccuracies Inherent in Patient-Specific Dual-Energy X-Ray Absorptiometry Bone Mineral Density Measurements: Comprehensive Phantom-Based Evaluation. Journal of Bone and Mineral Research, 16(2), Article 2. https://doi.org/10.1359/jbmr.2001.16.2.417

Bone Mass Measurement: What the Numbers Mean | NIH Osteoporosis and Related Bone Diseases National Resource Center. (2018). NIH Osteoporosis and Related Bone Diseases National Resource Center. https://www.bones.nih.gov/health-info/bone/bone-health/bone-mass-measure

Borrè, A., Boano, R., Di Stefano, M., Castiglione, A., Ciccone, G., Isaia, G. C., Panattoni, G. L., & Faletti, C. (2015). X-ray, CT and DXA study of bone loss on medieval remains from North-West Italy. La Radiologia Medica, 120(7), Article 7. https://doi.org/10.1007/s11547-015-0507-3

Brødholt, E. T., Günther, C.-C., Gautvik, K. M., Sjøvold, T., & Holck, P. (2021). Bone mineral density through history: Dual-energy X-ray absorptiometry in archaeological populations of Norway. Journal of Archaeological Science: Reports, 36, 102792. https://doi.org/10.1016/j.jasrep.2021.102792

Cameron, J. R., Mazess, R. B., & Sorenson, J. A. (1968). Precision and Accuracy of Bone Mineral Determination by Direct Photon Absorptiometry. Investigative Radiology, 3(3), 141–150.

Cameron, J. R., & Sorenson, J. (1963). Measurement of Bone Mineral in vivo: An Improved Method. Science, 142, 230–232. https://doi.org/10.1126/science.142.3589.230

Carrack | ship. (2016). Encyclopaedia Britannica. Retrieved 15 April 2021, from https://www.britannica.com/technology/carrack

Cohen, B., & Rushton, N. (1995). Accuracy of DEXA measurement of bone mineral density after total hip arthroplasty. The Journal of Bone and Joint Surgery. British Volume, 77-B(3), 479–483. https://doi.org/10.1302/0301-620X.77B3.7744941

Currey, J. D. (2003). The Many Adaptations of Bone. Journal of Biomechanics, 36(10), 1487–1495. https://doi.org/10.1016/S0021-9290(03)00124-6

DMS Imaging. (2016). Stratos dR. Retrieved May 24, 2021, from https://www.dms.com/en/stratos-dr-2/

DXA: The Gold Standard. (2022). Hologic DXA. https://dxaperformance.com/dxa-the-gold-standard/

El Maghraoui, A., & Roux, C. (2008). DXA scanning in clinical practice. QJM: An International Journal of Medicine, 101(8), 605–617. https://doi.org/10.1093/qjmed/hcn022

Fackler, M. L., & Malinowski, J. A. (1985). The wound profile: A visual method for quantifying gunshot wound components. The Journal of Trauma, 25(6), 522–529.

Frost, H. M. (1994). Wolff's Law and bone's structural adaptations to mechanical usage: An overview for clinicians. The Angle Orthodontist, 64(3), 175–188. https://doi.org/10.1043/0003-3219(1994)064<0175:WLABSA>2.0.CO;2

Glen, S. (2016). Measurement Error (Observational Error). Statistics How To. https://www.statisticshowto.com/measurement-error/

Gomez, F., Galvan, R. R., Cravioto, J., & Frenk, S. (1955). Malnutrition in Infancy and Childhood, with Special Reference to Kwashiorkor. Advances in Pediatrics, 7(1), 131–169. https://doi.org/10.1016/S0065-3101(22)00438-8

Griffiths, H. J. (1994). The Evaluation of Osteoporosis: Dual Energy X-ray Absorptiometry in Clinical Practice. Radiology, 192(2), 332–332. https://doi.org/10.1148/radiology.192.2.332

Hale, A. R., & Ross, A. H. (2018). Scanning Skeletal Remains for Bone Mineral Density in Forensic Contexts. Journal of Visualized Experiments, 131, Article 131. https://doi.org/10.3791/56713

Heale, R., & Twycross, A. (2015). Validity and reliability in quantitative studies. Evidence-Based Nursing, 18(3), 66–67. https://doi.org/10.1136/eb-2015-102129

Hologic QDR-4500C Elite—Bone Densitometer. (2015, January 4). Meditegic. http://localhost/hologic-qdr-4500c-elite-bone-den/

Hong, J., Hipp, J. A., Mulkern, R. V., Jaramillo, D., & Snyder, B. D. (2000). Magnetic resonance imaging measurements of bone density and cross-sectional

geometry. Calcified Tissue International, 66(1), 74–78. https://doi.org/10.1007/s002230050015

International Atomic Energy Agency (IAEA). (2017). Radiation protection of patients during DXA [Text]. IAEA. https://www.iaea.org/resources/rpop/health-professionals/other-specialities-and-imaging-modalities/dxa-bone-mineral-densitometry/patients

Kanis, J. A., Melton III, L. J., Christiansen, C., Johnston, C. C., & Khaltaev, N. (1994). The diagnosis of osteoporosis. Journal of Bone and Mineral Research, 9(8), 1137–1141. https://doi.org/10.1002/jbmr.5650090802

Keaveny, T. M. (2010). Biomechanical computed tomography—Noninvasive bone strength analysis using clinical computed tomography scans. Annals of the New York Academy of Sciences, 1192(1), 57–65. https://doi.org/10.1111/j.1749-6632.2009.05348.x

Kern. (2020). Precision Balances. Retrieved May 26, 2021, from https://www.kern-sohn.com/shop/en/laboratory-balances/precision-balances/PLS/PLJ/

Kraiger, M., Martirosian, P., Opriessnig, P., Eibofner, F., Rempp, H., Hofer, M., Schick, F., & Stollberger, R. (2012). A fully automated trabecular bone structural analysis tool based on T2*-weighted magnetic resonance imaging. Computerized Medical Imaging and Graphics, 36(2), 85–94. https://doi.org/10.1016/j.compmedimag.2011.07.006

Kranioti, E. F., Bonicelli, A., & García-Donas, J. G. (2019). Bone-mineral density: Clinical significance, methods of quantification and forensic applications. Research

and Reports in Forensic Medical Science, 9, 9–21. https://doi.org/10.2147/RRFMS.S164933

Langdahl, B., Ferrari, S., & Dempster, D. W. (2016). Bone modeling and remodeling: Potential as therapeutic targets for the treatment of osteoporosis. Therapeutic Advances in Musculoskeletal Disease, 8(6), 225–235. https://doi.org/10.1177/1759720X16670154

Li, X., Na, L., & Xiaoguang, C. (2014). Update on the Clinical Application of Quantitative Computed Tomography (QCT) in Osteoporosis. Current Radiology Reports, 2(10), 65. https://doi.org/10.1007/s40134-014-0065-9

Liu, Y.-L., Hsu, J.-T., Shih, T.-Y., Luzhbin, D., Tu, C.-Y., & Wu, J. (2018). Quantification of Volumetric Bone Mineral Density of Proximal Femurs Using a Two-Compartment Model and Computed Tomography Images. BioMed Research International, 2018, 6284269. https://doi.org/10.1155/2018/6284269

Ludbrook, J. (2013). Should we use one-sided or two-sided P values in tests of significance? Clinical and Experimental Pharmacology & Physiology, 40(6), 357–361. https://doi.org/10.1111/1440-1681.12086

Lunar iDXA. (2023). Retrieved 26 March 2023, from https://www.gehealthcare.com/products/bone-and-metabolic-health/lunar-idxa

Macchiarelli, R., & Bondioli, L. (1994). Linear densitometry and digital image processing of proximal femur radiographs: Implications for archaeological and forensic anthropology. American Journal of Physical Anthropology, 93(1), 109–122. https://doi.org/10.1002/ajpa.1330930108

Manske, S. L., Macdonald, H. M., Nishiyama, K. K., Boyd, S. K., & McKay, H. A. (2010). Clinical Tools to Evaluate Bone Strength. Clinical Reviews in Bone and Mineral Metabolism, 8(3), 122–134. https://doi.org/10.1007/s12018-009-9066-2

Marsden, P. R. V. (2015). Sealed by time: The loss and recovery of the Mary Rose. Oxbow Books.

Mazess, R. B., Barden, H. S., Bisek, J. P., & Hanson, J. (1990). Dual-energy x-ray absorptiometry for total-body and regional bone-mineral and soft-tissue composition. The American Journal of Clinical Nutrition, 51(6), 1106–1112. https://doi.org/10.1093/ajcn/51.6.1106

Mazess, R. B., Peppler, W. W., Harrison, J. E., & McNeill, K. G. (1981). Total body bone mineral and lean body mass by dual-photon absorptiometry. Calcified Tissue International, 33(1), 365–368. https://doi.org/10.1007/BF02409457

Meyer, U., Kruse-Lösler, B., & Wiesmann, H. P. (2006). Principles of bone formation driven by biophysical forces in craniofacial surgery. British Journal of Oral and Maxillofacial Surgery, 44(4), 289–295. https://doi.org/10.1016/j.bjoms.2005.06.026

Mishra, P., Pandey, C. M., Singh, U., Gupta, A., Sahu, C., & Keshri, A. (2019). Descriptive Statistics and Normality Tests for Statistical Data. Annals of Cardiac Anaesthesia, 22(1), 67–72. https://doi.org/10.4103/aca.ACA_157_18

MM Ingredients (2022). Pork Gelatine 240 Bloom. Retrieved May 20, 2022, from https://mmingredients.co.uk/product-category/gelatine/pork-gelatine-240-bloom/

Morgan, S. L., & Prater, G. L. (2017). Quality in dual-energy X-ray absorptiometry scans. Bone, 104, 13–28. https://doi.org/10.1016/j.bone.2017.01.033

Murray, A. (2022). How much ionising radiation is dangerous? https://research.csu.edu.au/integrity-ethics-compliance/radiation/forms-templates-proformas/radiation-life/ionising/how-much

Navega, D., Coelho, J. d'Oliveira, Cunha, E., & Curate, F. (2017). A New Method for Age at Death Estimation Based on Femoral Bone Mineral Density and Artificial Neural Networks. Journal of Forensic Sciences, 63(2), Article 2. https://doi.org/10.1111/1556-4029.13582

Ott, S. M., O'Hanlan, M., Lipkin, E. W., & Newell-Morris, L. (1997). Evaluation of vertebral volumetric vs. Areal bone mineral density during growth. Bone, 20(6), 553–556. https://doi.org/10.1016/S8756-3282(97)00057-4

PELI. (2022). Waterproof Protective Cases. Retrieved May 26, 2021, from https://peliproducts.co.uk/collections/cases

Poppe, J. (1992). Gelatin. In A. Imeson (Ed.), Thickening and Gelling Agents for Food (pp. 98–123). Springer US. https://doi.org/10.1007/978-1-4615-3552-2_5

Rachner, T. D., Khosla, S., & Hofbauer, L. C. (2011). Osteoporosis: Now and the future. The Lancet, 377(9773), 1276–1287. https://doi.org/10.1016/S0140-6736(10)62349-5

Radiology (ACR), R. S. of N. A. (RSNA) and A. C. of. (2022). Bone Densitometry (DEXA , DXA). Radiologyinfo.Org. https://www.radiologyinfo.org/en/info/dexa

Raising the Mary Rose. (2021). The Mary Rose. https://maryrose.org/recovering-the-mary-rose/

Reconstructing the crew of the Mary Rose. (2021). The Mary Rose. https://maryrose.org/news/reconstructing-the-crew-of-the-mary-rose/

Ruff, C. B., Holt, B. M., Niskanen, M., Sladek, V., Berner, M., Garofalo, E., ... & Tompkins, D. (2012). Stature and body mass estimation from skeletal remains in the European Holocene. American journal of physical anthropology, 148(4), 601-617.

Saps, M., Rosen, J. M., & Ecanow, J. (2014). X-ray detection of ingested non-metallic foreign bodies. World journal of clinical pediatrics, 3(2), 14.

Scorrer, J., Faillace, K. E., Hildred, A., Nederbragt, A. J., Andersen, M. B., Millet, M.-A., Lamb, A. L., & Madgwick, R. (n.d.). Diversity aboard a Tudor warship: Investigating the origins of the Mary Rose crew using multi-isotope analysis. Royal Society Open Science, 8(5), 202106. https://doi.org/10.1098/rsos.202106

Selvik, J. T., & Abrahamsen, E. B. (2017). On the meaning of accuracy and precision in a risk analysis context. Proceedings of the Institution of Mechanical Engineers, Part O: Journal of Risk and Reliability, 231(2), 91–100. https://doi.org/10.1177/1748006X16686897

Setiawati, R., & Rahardjo, P. (2018). Bone Development and Growth. In Osteogenesis and Bone Regeneration. IntechOpen. https://doi.org/10.5772/intechopen.82452

Shepherd, J., Ng, B., Sommer, M., & Heymsfield, S. B. (2017). Body Composition by DXA. Bone, 104, 101–105. https://doi.org/10.1016/j.bone.2017.06.010

Stirland, A. J. (2005). The Men of the Mary Rose: Raising the Dead. The History Press.

Stirland, A. J., & Waldron, T. (1997). Evidence for Activity Related Markers in the Vertebrae of the Crew of theMary Rose. Journal of Archaeological Science, 24(4), 329–335. https://doi.org/10.1006/jasc.1996.0117

Strauss, G., Hofer, M., Korb, W., Trantakis, C., Winkler, D., Burgert, O., Schulz, T., Dietz, A., Meixensberger, J., & Koulechov, K. (2006). Accuracy and precision in the evaluation of computer assisted surgical systems. A definition. HNO, 54(2), 78–84. https://doi.org/10.1007/s00106-005-1321-3

Sutlovic, D., Boric, I., Sliskovic, L., Popovic, M., Knezovic, Z., Nikolic, I., Vucinovic, A., & Vucinovic, Z. (2016). Bone mineral density of skeletal remains: Discordant results between chemical analysis and DXA method. Legal Medicine, 20, 18–22. https://doi.org/10.1016/j.legalmed.2016.03.008

Suzuki, T., Shimoda, T., Takahashi, N., Tsutsumi, K., Samukawa, M., Yoshimura, S., & Ogasawara, K. (2018). Factors affecting bone mineral density among snowy region residents in Japan: analysis using multiple linear regression and Bayesian network model. Interactive journal of medical research, 7(1), e8555.

Taylor, S. C., Hammer, N., Zwirner, J., Ondruschka, B., & Kieser, D. C. (2020). Morphometric and density comparisons of Bos taurus scapulae as a proxy to human frontal crania. Egyptian Journal of Forensic Sciences, 10(1), Article 1. https://doi.org/10.1186/s41935-020-00191-6

Teichtahl, A. J., Wluka, A. E., Wijethilake, P., Wang, Y., Ghasem-Zadeh, A., & Cicuttini, F. M. (2015). Wolff's law in action: A mechanism for early knee osteoarthritis. Arthritis Research & Therapy, 17(1), 207. https://doi.org/10.1186/s13075-015-0738-7

The British Library. (2023). The Anthony Roll | The British Library. https://www.bl.uk/collection-items/the-anthony-roll

The History of the Mary Rose. (2021). The Mary Rose. https://maryrose.org/the-history-of-the-mary-rose/

Tikkanen. (2021). Mary Rose | Description, Sinking, Salvage, & Facts. Encyclopedia Britannica. https://www.britannica.com/topic/Mary-Rose-English-warship

Wahner, H. W., Dunn, W. L., Brown, M. L., Morin, R. L., & Riggs, B. L. (1988). Comparison of Dual-Energy X-Ray Absorptiometry and Dual Photon Absorptiometry for Bone Mineral Measurements of the Lumbar Spine. Mayo Clinic Proceedings, 63(11), 1075–1084. https://doi.org/10.1016/S0025-6196(12)65502-5

Wertman. (2015). Archery in Tudor England. Janet Wertman. https://janetwertman.com/2015/09/29/archery-in-tudor-england/

What does blooming gelatine mean and how do you bloom gelatine. (2018). MM Ingredients. https://mmingredients.co.uk/blooming-gelatine/

Why did the Mary Rose sink? (2021). The Mary Rose. https://maryrose.org/why-did-the-mary-rose-sink/